

Unsteady turbulent buoyant plumes

M. J. Woodhouse^{1,2,†}, J. C. Phillips² and A. J. Hogg¹

¹School of Mathematics, University of Bristol, University Walk, Bristol BS8 1TW, UK

²School of Earth Science, University of Bristol, Wills Memorial Building, Queen's Road, Bristol BS8 1RJ, UK

(Received 29 May 2015; revised 23 October 2015; accepted 4 February 2016;
first published online 5 April 2016)

We model the unsteady evolution of turbulent buoyant plumes following temporal changes to the source conditions. The integral model is derived from radial integration of the governing equations expressing the evolution of mass, axial momentum and buoyancy in the plume. The non-uniform radial profiles of the axial velocity and density deficit in the plume are explicitly captured by shape factors in the integral equations; the commonly assumed top-hat profiles lead to shape factors equal to unity. The resultant model for unsteady plumes is hyperbolic when the momentum shape factor, determined from the radial profile of the mean axial velocity in the plume, differs from unity. The solutions of the model when source conditions are maintained at constant values are shown to retain the form of the well-established steady plume solutions. We demonstrate through a linear stability analysis of these steady solutions that the inclusion of a momentum shape factor in the governing equations that differs from unity leads to a well-posed integral model. Therefore, our model does not exhibit the mathematical pathologies that appear in previously proposed unsteady integral models of turbulent plumes. A stability threshold for the value of the shape factor is also identified, resulting in a range of its values where the amplitudes of small perturbations to the steady solutions decay with distance from the source. The hyperbolic character of the system of equations allows the formation of discontinuities in the fields describing the plume properties during the unsteady evolution, and we compute numerical solutions to illustrate the transient development of a plume following an abrupt change in the source conditions. The adjustment of the plume to the new source conditions occurs through the propagation of a pulse of fluid through the plume. The dynamics of this pulse is described by a similarity solution and, through the construction of this new similarity solution, we identify three regimes in which the evolution of the transient pulse following adjustment of the source qualitatively differs.

Key words: plumes/thermals, turbulent convection

1. Introduction

Turbulent buoyant plumes occur in numerous industrial and environmental settings (Woods 2010; Hunt & van den Bremer 2011). Industrial examples include ventilation

† Email address for correspondence: mark.woodhouse@bristol.ac.uk

and heating (e.g. Baines & Turner 1969; Linden, Lane-Serff & Smeed 1990; Shrinivas & Hunt 2014), industrial chimneys (e.g. Slawson & Csanady 1967) and waste-water disposal (e.g. Koh & Brooks 1975). In the natural environment, turbulent plumes are found in meteorological (e.g. Emanuel 1994; Stevens 2005), oceanographical (e.g. Speer & Rona 1989; Straneo & Cenedese 2015) and volcanological (e.g. Woods 1988; Sparks *et al.* 1997; Woodhouse *et al.* 2013) settings. Models of steady plumes, based on the integral modelling approach pioneered by Zeldovich (1937), Schmidt (1941), Rouse, Yih & Humphreys (1952), Priestley & Ball (1955) and Morton, Taylor & Turner (1956), have been applied extensively to understand plume dynamics. In this approach, the turbulent flow in the plume is described on a time scale that is longer than the eddy turnover time (the time scale that characterizes the turbulent motion), and therefore the complicated turbulent motions are not explicitly modelled and only the evolution of mean flow quantities with distance from the source is modelled. A further simplification is obtained by integrating the mean flow quantities over the cross-section of the plume, resulting in a system of nonlinear ordinary differential equations that describe the spatial development of the steady integral flow quantities such as the fluxes of mass, momentum and buoyancy.

To obtain the integral fluxes, it is necessary to specify the radial and azimuthal dependence of the three-dimensional mean fields. When the flow domain and ambient conditions do not introduce an asymmetry, the time-averaged flow quantities are axisymmetric and swirl-free (i.e. there is no azimuthal dependence of the mean flow quantities). Experiments suggest that, at sufficiently high Reynolds number and for an unstratified ambient fluid, buoyant plumes attain self-similar radial profiles for both the mean axial velocity and the concentration of the species that gives rise to the density difference between the plume and the ambient fluid sufficiently far from the fluid source (Papanicolaou & List 1988; Shabbir & George 1994; Wang & Law 2002; Ezzamel, Salizzoni & Hunt 2015). Furthermore, higher-order turbulent quantities such as the turbulent intensity (the root mean square of velocity component fluctuations and concentration fluctuations from the mean) and turbulent stresses also evolve with self-similar radial profiles (Papanicolaou & List 1988; Wang & Law 2002; Ezzamel *et al.* 2015). The cross-sectional integration then results in a system of ordinary differential equations that models the evolution of the mass flux, momentum flux and buoyancy flux with distance from the source. For stratified ambient environments, the detailed structure and evolution of the mean and turbulent quantities have been scrutinized less thoroughly. However, the applicability of integral models assuming similarity of the mean flow profiles has been demonstrated through comparison of model predictions with laboratory experiments (see, e.g., Morton *et al.* 1956; List 1982) and in field-scale applications (see, e.g., Turner 1986; Woods 1988; Speer & Rona 1989; Kaye 2008).

While averaging over the turbulent time scale and integrating over the plume cross-section significantly simplifies the mathematical description of the plume dynamics, detailed information about the turbulent flow is not fully captured. The integral model of Morton *et al.* (1956) incorporates the turbulent nature of the flow through a parameterization of turbulent mixing as an inflow of fluid from the ambient to the plume, referred to as entrainment. The velocity of the entraining flow is linearly related to the mean axial velocity scale of the plume (as dimensional analysis demands, since the only velocity scale that remains following time-averaging and cross-sectional integration is the mean axial velocity of the plume). Morton *et al.* (1956) take a constant entrainment coefficient, and the application of this model has been successful in describing steady buoyant plumes over a wide range of scales,

from the laboratory (see, e.g., Morton *et al.* 1956; List 1982) to plumes from large volcanic eruptions (e.g. Woods 1988), illustrating the success of the integral modelling approach with a constant entrainment coefficient.

Detailed examination of laboratory experiments of turbulent plumes suggests that the entrainment coefficient does not have a constant universal value, but rather evolves as the flow develops (Wang & Law 2002; Kaminski, Tait & Carazzo 2005; Ezzamel *et al.* 2015). In particular, for plumes that are strongly forced with a flux of momentum at the source (referred to as buoyant jets), the entrainment coefficient transitions from a value appropriate for jets to the value for plumes as the flow becomes increasingly driven by buoyancy. Integral models that include an evolving entrainment coefficient have been proposed (see, e.g., Fox 1970; Kaminski *et al.* 2005; Carazzo, Kaminski & Tait 2006; Craske & van Reeuwijk 2015*a,b*), building on the integral modelling approach of Priestley & Ball (1955) whereby an integral expression for the conservation of axial kinetic energy is used with conservation of momentum to derive an integral expression for conservation of mass. (This modelling approach is discussed further in appendix A.) However, the assumption of a constant entrainment coefficient captures the leading-order behaviour of turbulent buoyant plumes over a wide range of scales (Turner 1986), and for fully developed turbulent plumes sufficiently far from the source, a constant entrainment coefficient is appropriate and represents the similarity of the flow profiles and the turbulent entrainment processes at different heights in the plume (Turner 1986; Ezzamel *et al.* 2015).

The applicability of steady models to the inherently unsteady turbulent motion relies on a separation of time scales. If the conditions at the plume source and in the ambient are held steady, the steady integral models describe the plume behaviour well on time scales that are long compared with the eddy turnover time (Woods 2010). However, if the source conditions change on a time scale that is longer than the turbulent fluctuations, then a signature of the source variation may be seen in the time-averaged plume dynamics downstream of the source (e.g. Scase, Caulfield & Dalziel 2008; Scase 2009). Unsteady sources occur frequently in natural settings, for example as the strength of a volcanic source changes in magnitude during an eruption. In addition, temporal changes in ambient conditions on a time scale similar to the ascent time of a fluid parcel are likely to result in a transient response of the plume.

To model unsteady plumes, integral models have been proposed (Delichatsios 1979; Yu 1990; Vul'fson & Borodin 2001; Scase, Caulfield & Dalziel 2006*a*; Scase *et al.* 2006*b*, 2008; Scase 2009; Scase, Aspden & Caulfield 2009) which extend the modelling approach of Morton *et al.* (1956) while retaining some of the underlying assumptions of the steady model. In particular, the unsteady models capture the variations of flow quantities on a time scale that is longer than the eddy turnover time, and assume that the radial profiles of the mean axial velocity and the concentration of the buoyancy-generating species remain in a self-similar form throughout the evolution. However, given the difficulty in obtaining robust experimental results for plumes with time-varying source conditions, the underlying assumptions have yet to be scrutinized in detail. Numerical simulation of the governing equations can be used as a surrogate for laboratory experiments and allow detailed investigations of the turbulent flow properties throughout the modelled domain (Jiang & Luo 2000; Plourde *et al.* 2008; Craske & van Reeuwijk 2013, 2015*a*). The physical basis of this class of unsteady models has been further questioned by Scase & Hewitt (2012) in an analysis of the stability of the steady solutions of the models of Delichatsios (1979), Yu (1990) and Scase *et al.* (2006*b*) to small harmonic perturbations at the

source. Scase & Hewitt (2012) find that the perturbations grow as they propagate through the plume, and that the growth rate increases without bound as the frequency of the source oscillations is increased; therefore the models are ill-posed, suggesting that a critical physical process has been neglected (Joseph & Saut 1990).

In an attempt to ‘regularize’ the unsteady plume models, Scase & Hewitt (2012) introduce a phenomenological diffusive term to represent turbulent mixing processes into the equation that expresses the balance of axial momentum; it curtails the unbounded growth of short-wavelength perturbations, thus leading to a well-posed model. The form of the diffusive term has been investigated by Craske & van Reeuwijk (2015a) for momentum-driven (non-buoyant) jets using direct numerical simulations; the numerical simulations suggest that the diffusive term proposed by Scase & Hewitt (2012) does not describe the transient evolution of momentum-driven jets well. Here, we find that the diffusive term introduced by Scase & Hewitt (2012) leads to a new pathology in the system of equations; the steady states of the ‘regularized’ model are spatially unstable and therefore cannot be realized.

We show here that the ill-posedness in the unsteady models analysed by Scase & Hewitt (2012) is due to the assumption of a top-hat profile for the mean axial velocity (i.e. the axial velocity at any height is assumed to be radially invariant within the plume and zero outside of the plume) and therefore a failure to account for the non-uniform radial profile of the mean axial velocity of the plume. Non-uniform radial profiles for the axial velocity were examined in the early studies of steady plumes by Priestley & Ball (1955) and Morton *et al.* (1956). However, solutions of steady plume models have the same form whether top-hat or non-uniform radial profiles for the mean axial velocity are adopted, as dimensional analysis demands, with only changes to coefficients in the solutions (Morton *et al.* 1956; Linden 2000; Kaye 2008), and many subsequent analyses of steady plumes have adopted the top-hat formulation.

When a top-hat velocity profile is adopted, the cross-sectionally averaged mass and momentum of the plume are transported with the same rate, but the transport rates differ when the radial profile of the mean axial velocity is non-uniform. We therefore propose an integral model of unsteady plumes that explicitly accounts for the different transport rates of the cross-sectionally averaged mass and axial momentum of the plume, by introducing a ‘shape factor’ in the equation for the conservation of momentum that differs from unity when non-uniform radial profiles of the mean axial velocity are assumed. A shape factor that differs from unity in shallow-water hydraulic models has been shown to fundamentally alter solutions of the system of equations due to a change in the characteristics of the hyperbolic system (Hogg & Pritchard 2004). Here, we show that the inclusion of a shape factor changes the character of the system of equations describing unsteady plumes and leads to a well-posed system of equations without the need to include diffusive terms.

A similar approach to regularizing an unsteady integral model of momentum-driven jets has been proposed recently by Craske & van Reeuwijk (2015a,b). Through analysis of their direct numerical simulations, Craske & van Reeuwijk (2015a,b) develop a well-posed integral model of unsteady jets that includes a description of dispersion in the jet, resulting from the non-uniform radial profile of the mean axial velocity which leads to different transport rates for mass, axial momentum and kinetic energy (referred to as type I dispersion by Craske & van Reeuwijk 2015a,b), and the deviation of the radial profile of mean axial velocity from a self-similar form (referred to as type II dispersion). Type II dispersion is important in jets, where the flow structure evolves significantly in the neighbourhood of the source even for temporally invariant source conditions (Wang & Law 2002; Kaminski *et al.* 2005;

Ezzamel *et al.* 2015), but is likely to be less important for fully developed turbulent plumes for which the radial profiles are in self-similar forms (Ezzamel *et al.* 2015). However, Craske & van Reeuwijk (2015*a,b*) show that explicitly accounting for the non-uniform radial profile of mean axial velocity (type I dispersion) in the integral equations is critical to the well-posedness of the unsteady integral model for jets.

In this paper we demonstrate, through an analysis of the temporal evolution of small perturbations to steady solutions, that an integral model of unsteady plumes is well-posed when the momentum shape factor differs from unity. Furthermore, we identify a stability threshold in the value of the shape factor above which the amplitude of small perturbations decays. The system of equations we propose is hyperbolic, with a characteristic structure that, in certain situations, allows for the formation of ‘shocks’ during the transient evolution. Through the construction of similarity solutions, we identify scaling relationships that capture the propagation and growth of a transient pulse that is advected through the plume following an abrupt change in the source conditions, and determine the regimes in which shocks are formed.

This paper is organized as follows. In § 2 we provide a derivation of an integral model of unsteady buoyant plumes, and we demonstrate that the use of integral flow quantities requires the inclusion of shape factors for the transport rates of the (cross-sectionally averaged) axial momentum and buoyancy of the plume. We show that a momentum shape factor only slightly modifies the classical power-law solutions of Morton *et al.* (1956). In § 3 we re-examine the phenomenological diffusive term introduced by Scase & Hewitt (2012), and show that this model potentially introduces a new pathology into the system of equations whereby steady solutions are spatially unstable. We therefore examine the mathematical structure and well-posedness of an unsteady integral model for plumes that includes a momentum shape factor, and we demonstrate in § 4 that this leads to a well-posed system of equations. Numerical solutions of our unsteady model are presented in § 5 to support the mathematical analysis. In § 6 we consider the evolution of a plume following an abrupt change in the source buoyancy flux and show that the adjustment of the plume occurs through the propagation of a pulse whose dynamics is described by a similarity solution. Finally, in § 7 we discuss the implications of our mathematical model and draw our conclusions.

2. An integral model for unsteady turbulent buoyant plumes

We model an unsteady turbulent buoyant plume formed due to the release of a fluid from a point source into an otherwise quiescent ambient fluid of a different density. A cylindrical coordinate system is adopted, with \hat{r} and \hat{z} denoting unit vectors in the radial and vertical directions respectively. The plume and ambient are composed of incompressible fluids, and the plume is assumed to have a circular (time-averaged) cross-section. The velocity field, \mathbf{u} , is assumed to be axisymmetric, with $\mathbf{u} = u\hat{r} + w\hat{z}$. We further assume that the plume is slender (as observed in experiments, e.g. Rouse *et al.* 1952), such that $R/H \ll 1$, where R and H denote typical length scales in the radial and vertical directions respectively, that the Reynolds number of the emitted fluid at the source is sufficiently high, such that the turbulent motion is fully developed throughout the flow domain, and that the plume fluid transports a scalar species (such as heat or salt) with the plume density linearly related to the concentration of the species.

Turbulence in the plume is responsible for the entrainment of ambient fluid and mixing of the plume and ambient fluids, and its role is central to the ensuing

dynamics. We therefore adopt the Reynolds-averaged Navier–Stokes equations to describe the fluid motion, with a Reynolds-averaged advection–diffusion equation to describe the transport of the scalar species that results in the density difference between the plume and the ambient fluids, taking $u = \bar{u} + u'$, $w = \bar{w} + w'$ and $g_r = \bar{g}_r + g_r'$, where \bar{u} and u' denote the ensemble average and the fluctuation about the average of u respectively, and similarly for w and g_r , and where $g_r = g(\rho_a - \rho)/\rho_0$ is the reduced gravity, with g denoting the gravitational acceleration, ρ and ρ_a denoting the density of the plume and ambient fluids respectively, and ρ_0 being a characteristic density scale. The equations for the conservation of (the ensemble averaged) mass, axial momentum and reduced gravity are then

$$\frac{1}{r} \frac{\partial}{\partial r} (r\bar{u}) + \frac{\partial \bar{w}}{\partial z} = 0, \quad (2.1a)$$

$$\frac{\partial \bar{w}}{\partial t} + \frac{1}{r} \frac{\partial}{\partial r} (r\bar{u}\bar{w}) + \frac{\partial}{\partial z} (\bar{w}^2) = \bar{g}_r - \frac{1}{r} \frac{\partial}{\partial r} (r\overline{u'w'}) - \frac{\partial}{\partial z} (\overline{w'^2}), \quad (2.1b)$$

$$\frac{\partial \bar{g}_r}{\partial t} + \frac{1}{r} \frac{\partial}{\partial r} (r\bar{g}_r\bar{u}) + \frac{\partial}{\partial z} (\bar{g}_r\bar{w}) = \frac{g}{\rho_0} \left(\frac{\partial \rho_a}{\partial t} + \frac{\partial}{\partial z} (\bar{w}\rho_a) \right) - \frac{1}{r} \frac{\partial}{\partial r} (r\overline{g_r'u'}) - \frac{\partial}{\partial z} (\overline{g_r'w'}). \quad (2.1c)$$

It should be noted that in (2.1) the slenderness of the plume has been used to simplify the Reynolds-averaged Navier–Stokes equations, as described for steady plumes by Linden (2000). In particular, the radial momentum balance (not given) shows that, to leading order in the plume slenderness, there is no radial pressure gradient. Therefore, the pressure in the plume can be taken to be equal to the hydrostatic pressure of the ambient. We have also invoked the Boussinesq approximation whereby differences in density are sufficiently small that they may be neglected except where they are multiplied by the gravitational acceleration. Furthermore, we have neglected molecular diffusion terms under the assumption that the Reynolds number and Péclet number are sufficiently large that mixing is dominantly due to turbulence.

Integral equations are obtained by integrating each of equations (2.1) over a cross-section of the plume. We define a surface $r = b(z, t)$ representing the boundary of the plume over which entrainment of ambient fluid into the plume occurs, and impose the boundary condition on this surface,

$$\bar{u}(b, z, t) = \frac{\partial b}{\partial t} + \bar{w}(b, z, t) \frac{\partial b}{\partial z} + u_e, \quad (2.2)$$

where the entrainment velocity, u_e , is the radial velocity of the ambient fluid across $r = b(z, t)$ (note that $u_e < 0$ when ambient fluid is entrained into the plume). This boundary condition represents the advection of the surface with the local velocity of the plume, with entrainment represented as a sink of mass (equivalently volume under the Boussinesq approximation), with the volume flux per unit area of the surface across $r = b(z, t)$ given by u_e . We note that this approach differs from that taken by Craske & van Reeuwijk (2015a,b), who adopt the characteristic length and velocity scales defined through the cross-sectionally averaged fluxes of mass and axial momentum which themselves are defined in terms of an additional length scale at which the mean axial velocity can be considered negligible in contrast to the mean axial velocity at the centreline. As turbulent plumes typically exhibit non-uniform radial profiles of axial velocity and concentration of species, with decaying velocity and concentration with the radial distance from the plume axis, in

laboratory experiments or direct numerical simulations there is a choice as to how to define the plume edge, taking, for examples, the radial distance at which the axial velocity or concentration reaches a specified threshold, or the radial distance at which the mass flux included in a cross-sectional integral captures a specified proportion of the total mass flux induced by the plume. We discuss below how these choices are represented in our model.

Integration of the point-wise conservation equation (2.1) over a plume cross-section, using Leibniz’s theorem for interchanging differentiation and integration (Flanders 1973) together with the boundary condition (2.2), gives

$$b \frac{\partial b}{\partial t} + \frac{\partial}{\partial z} \int_0^b r \bar{w} dr = -bu_e, \tag{2.3a}$$

$$\begin{aligned} \frac{\partial}{\partial t} \int_0^b r \bar{w} dr + \frac{\partial}{\partial z} \int_0^b r \bar{w}^2 dr &= \int_0^b r \bar{g}_r dr - \frac{\partial}{\partial z} \int_0^b r \bar{w}^2 dr \\ &- b \bar{w}(b, z, t) u_e - b \bar{w}'(b, z, t) + b \bar{w}^2(b, z, t) \frac{\partial b}{\partial z}, \end{aligned} \tag{2.3b}$$

$$\begin{aligned} \frac{\partial}{\partial t} \int_0^b r \bar{g}_r dr + \frac{\partial}{\partial z} \int_0^b r \bar{w} \bar{g}_r dr &= \frac{g}{\rho_0} \int_0^b \left(\frac{\partial \rho_a}{\partial t} + \bar{w} \frac{\partial \rho_a}{\partial z} \right) r dr \\ &- \frac{\partial}{\partial z} \int_0^b r \bar{g}'_r \bar{w}' dr - b \bar{g}'_r(b, z, t) u_e - b \bar{w}' \bar{g}'_r(b, z, t) - b \bar{w}' \bar{g}'_r(b, z, t) \frac{\partial b}{\partial z}, \end{aligned} \tag{2.3c}$$

representing the evolution of mass, momentum and buoyancy respectively.

We define the integral volume flux as $Q = b^2 W$ (note that, under the Boussinesq assumption, Q can also be referred to as the (specific) mass flux), the (specific) momentum flux as $M = b^2 W^2$ and the buoyancy flux as $F = b^2 W G'$. Here, W and G' denote the cross-sectionally averaged mean axial velocity and the reduced gravity of the plume respectively, and are given by

$$W = \frac{2}{b^2} \int_0^b r \bar{w} dr, \quad \text{and} \quad G' = \frac{2}{b^2} \int_0^b r \bar{g}_r dr. \tag{2.4a,b}$$

We then have

$$\int_0^b r \bar{w}^2 dr = \frac{1}{2} S_m M \quad \text{and} \quad \int_0^b r \bar{w} \bar{g}_r dr = \frac{1}{2} S_f F, \tag{2.5a,b}$$

where S_m and S_f are momentum and buoyancy ‘shape factors’ respectively, defined as

$$S_m(z, t) = 1 + \frac{2}{b^2 W^2} \int_0^b r (\bar{w} - W)^2 dr \tag{2.6}$$

and

$$S_f(z, t) = 1 + \frac{2}{b^2 W G'} \int_0^b r (\bar{w} - W)(\bar{g}_r - G') dr. \tag{2.7}$$

Thus, the shape factors quantify the effect of non-uniform radial profiles of the axial velocity and density on the rates of transport of momentum and scalar species. Crucially, we note that $S_m \geq 1$, which is representative of the more rapid transport

of momentum than mass in the plume, unless the mean axial velocity is radially invariant within the plume (in which case $S_m \equiv 1$ and $S_f \equiv 1$). It should be noted that this latter condition occurs only for ‘top-hat’ profiles as described below.

The plume edge, given by the surface $r = b(z, t)$, is chosen to be at a radial distance such that the boundary terms in (2.3) are negligible in comparison to the integral terms (e.g. $\bar{w}(b) \ll W$, $\overline{u'w'}(b) \ll W^2$, etc.). Furthermore, the entrainment assumption of Morton *et al.* (1956) allows the entrainment velocity to be written as $u_e = -\alpha W$, where α is the entrainment coefficient. This simplification of the turbulence mixing dynamics assumes a similarity of turbulent structures at each height in the plume. The entrainment coefficient must be determined empirically and, for fully developed plumes far from the source where the radial profiles of the axial velocity have a self-similar Gaussian form, a constant value $\alpha = 0.1 \pm 0.01$ is appropriate (Morton *et al.* 1956; List 1982; Woods 2010). However, near to the source (or for non-ideal initial conditions), the entrainment coefficient may vary substantially as the flow develops (Wang & Law 2002; Kaminski *et al.* 2005; Ezzamel *et al.* 2015). In this study we take a constant entrainment coefficient, with the exception of appendix A, where we also examine the steady solutions of a model with an entrainment coefficient that varies as the flow develops.

We note from (2.6) that the value of the momentum shape factor is tied to the choice of the plume width, $b(z, t)$. If we assume that the mean axial velocity has a self-similar Gaussian profile in the radial direction, as inferred from laboratory experiments on steady plumes (Papanicolaou & List 1988; Shabbir & George 1994), so that the mean axial velocity of the plume can be written as

$$\bar{w}(r, z, t) = \bar{W}(z, t)e^{-r^2/R^2}, \quad (2.8)$$

where $\bar{W}(z, t)$ is the mean axial velocity on the plume axis and $R(z, t)$ is a characteristic length scale for radial variation determined from observations, then the shape factor is given by

$$S_m = \frac{b^2(1 + e^{-b^2/R^2})}{2R^2(1 - e^{-b^2/R^2})}. \quad (2.9)$$

The plume width can be related to the length scale of the Gaussian radial profile $R(z, t)$ through a threshold on the mean axial velocity. For example, Morton *et al.* (1956) and Papanicolaou & List (1988) define the characteristic length scale of a Gaussian plume as the radial position at which the axial velocity is a factor of $1/e$ of the centreline value (i.e. $b = R$), and this results in $S_m = 1.08$.

The entrainment hypothesis and the use of shape factors for the integral fluxes of momentum and buoyancy allow the integral conservation equation (2.3) to be written in terms of the integral fluxes of volume, momentum and buoyancy as

$$\frac{\partial}{\partial t} \left(\frac{Q^2}{M} \right) + \frac{\partial Q}{\partial z} = 2\alpha\sqrt{M}, \quad (2.10a)$$

$$\frac{\partial Q}{\partial t} + \frac{\partial}{\partial z} (S_m M) = \frac{QF}{M} - \frac{\partial}{\partial z} \int_0^b 2r\overline{w'^2} dr, \quad (2.10b)$$

$$\frac{\partial}{\partial t} \left(\frac{QF}{M} \right) + \frac{\partial}{\partial z} (S_f F) = \frac{b^2 g}{\rho_0} \left(\frac{\partial \rho_a}{\partial t} + W \frac{\partial \rho_a}{\partial z} \right) - \frac{\partial}{\partial z} \int_0^b 2r\overline{g'_r w'} dr. \quad (2.10c)$$

While the system (2.10) applies to a spatially and temporally varying ambient density field, for the remainder of this study we consider plumes in an unstratified ambient, with ρ_a constant. The shape factors S_m and S_f could be spatially and temporally varying, as the radial profiles of the axial plume velocity and reduced gravity evolve (Carazzo *et al.* 2006; Craske & van Reeuwijk 2015a,b; Ezzamel *et al.* 2015). However, for fully developed plumes, laboratory experiments suggest that the axial plume velocity and reduced gravity attain self-similar forms (Morton *et al.* 1956; Papanicolaou & List 1988; Shabbir & George 1994; Ezzamel *et al.* 2015), such that the shape factors can be taken to be constants. While temporal changes in the source conditions could result in local variations in the shape factors, we expect the contribution of that change to be small. Therefore, here we consider the simplest case of $S_m = S$ with S constant and $S_f \equiv 1$ to investigate the structure of the model, but note that we would expect that S_f differs from unity. For example, taking a Gaussian profile for the reduced gravity, $\overline{g_r}(r, z, t) = \overline{G_r}(z, t)e^{-r^2/\lambda^2 R^2}$, where $\overline{G_r}(z, t)$ is the centreline value and $\lambda \approx 1.2$ (Papanicolaou & List 1988), we find $S_f = 1.06$ when taking $b = R$. However, it will be shown below that it is the divergence of the momentum shape factor, S_m , from unity that makes the significant difference to the model system (2.10), changing it from parabolic for $S_m = 1$ to hyperbolic for $S_m > 1$, whereas the buoyancy shape factor plays a less significant role, only leading to loss of hyperbolicity if $S_f = S_m \pm \sqrt{S_m^2 - S_m}$ (see § 4).

In the integral equations for conservation of momentum (2.10b) and conservation of buoyancy (2.10c) we have retained integral terms that represent turbulent axial diffusion of momentum and buoyancy respectively. Typically, in steady plume models these diffusive terms have been neglected (we refer to the system of integral equations (2.10) without the turbulent diffusive terms as the ‘non-diffusive’ system). Indeed, Morton (1971) argues that

$$\frac{\partial}{\partial z}(\overline{w'^2}) \ll \frac{1}{r} \frac{\partial}{\partial r}(r\overline{w'w'}) \quad \text{and} \quad \frac{\partial}{\partial z}(\overline{w'g_r'}) \ll \frac{1}{r} \frac{\partial}{\partial r}(r\overline{w'g_r'}), \tag{2.11a,b}$$

and therefore the contributions of the turbulent diffusion terms to the plume dynamics are of a similar magnitude to boundary terms which are neglected. We note that some studies on momentum-driven jets from maintained sources retain the axial derivatives of quadratic fluctuation terms to model the contribution of a non-hydrostatic axial pressure gradient (see, e.g., Shabbir & George 1994; Wang & Law 2002; Yannopoulos 2006). When these turbulent diffusion terms are neglected, the momentum shape factor is taken to be constant ($S_m = S$ with S constant), the buoyancy shape factor $S_f \equiv 1$ and the ambient fluid is unstratified, the governing equations (2.10) can be written as

$$\frac{\partial}{\partial t} \left(\frac{Q^2}{M} \right) + \frac{\partial Q}{\partial z} = 2\alpha\sqrt{M}, \tag{2.12a}$$

$$\frac{\partial Q}{\partial t} + S \frac{\partial M}{\partial z} = \frac{QF}{M}, \tag{2.12b}$$

$$\frac{\partial}{\partial t} \left(\frac{QF}{M} \right) + \frac{\partial F}{\partial z} = 0. \tag{2.12c}$$

The steady integral equations with pure-plume boundary conditions ($Q = 0, M = 0, F = F_0$ at $z = 0$) have well-known power-law solutions (Morton *et al.* 1956), and

these solutions are little altered by the momentum shape factor; for $S \geq 1$ the steady solutions of the non-diffusive system of equation (2.12) are

$$Q = Q_0(z) = q_0 z^{5/3}, \quad M = M_0(z) = m_0 z^{4/3}, \quad F = F_0, \quad (2.13a-c)$$

where

$$q_0 = \frac{6\alpha}{5} \left(\frac{9\alpha}{10}\right)^{1/3} \left(\frac{F_0}{S}\right)^{1/3}, \quad m_0 = \left(\frac{9\alpha}{10}\right)^{2/3} \left(\frac{F_0}{S}\right)^{2/3}. \quad (2.14a,b)$$

In the top-hat limit $S \rightarrow 1$ the solution of Morton *et al.* (1956) is recovered. Furthermore, the effective radius of the plume, $b_0(z) = Q_0/\sqrt{M_0} = 6\alpha z/5$, is independent of the shape factor. Therefore, the momentum shape factor cannot be determined from measurement of the plume radius alone, in contrast to the entrainment coefficient which can be determined using the spreading rate of the steady plume.

Scase & Hewitt (2012) advocate modelling of the turbulent diffusion terms (particularly the diffusion of momentum) in (2.10) in the unsteady plume model to obtain a well-posed system of equations. Recently, Craske & van Reeuwijk (2015a,b) have demonstrated the relatively weak role of turbulent diffusion for momentum-driven jets, but that diffusive effects in the jet occur due to the departure of flow variables from self-similar forms (type II dispersion in the nomenclature of Craske & van Reeuwijk 2015a,b). However, we suggest that the dominant dynamics for turbulent plumes can be described by the non-diffusive system of equations. Indeed, we show below that the inclusion of diffusive terms modelling turbulent diffusion can lead to difficulties in the integral model. We therefore analyse the non-diffusive system and show that a momentum shape factor that differs from unity is sufficient to obtain a well-posed model.

3. Difficulties associated with the turbulent diffusive terms

In an analysis of a non-diffusive unsteady plume model with shape factors $S \equiv 1$ and $S_f \equiv 1$, corresponding to top-hat radial profiles for the axial velocity and reduced gravity (i.e. \bar{w} and \bar{g}_r are radially invariant for $r \leq b$ and equal to zero for $r > b$), Scase & Hewitt (2012) assess the well-posedness of the system of equations by introducing small harmonic perturbations to the source buoyancy flux, and examine the growth of the perturbations downstream of the source. A linear analysis shows that the perturbations grow with distance from the source, indicating instability, and, more importantly, the growth rate of the perturbations increases without bound as the frequency of the harmonic oscillation of the source buoyancy flux increases (Scase & Hewitt 2012). The non-diffusive system of equations with $S \equiv 1$ and $S_f \equiv 1$ is therefore ill-posed, as there is a loss of continuous dependence of the solution on the boundary conditions (Joseph & Saut 1990; Scase & Hewitt 2012). The ill-posedness is manifested in numerical solutions of the system of equations by an inability to compute solutions that are independent of the truncation implicit in the numerical scheme (e.g. grid-scale dependence for finite-difference methods).

The ill-posedness identified by Scase & Hewitt (2012) in the non-diffusive system when top-hat profiles are assumed (i.e. when $S \equiv 1$) may be due to a missing physical process that provides a mechanism to curtail the unbounded growth of the arbitrarily short-wavelength/high-frequency modes (Joseph & Saut 1990; Scase & Hewitt 2012). In an attempt to regularize the ill-posed system, Scase & Hewitt (2012) introduce

a phenomenological model for the diffusive term in the momentum balance (2.10b), appealing to Prandtl’s mixing-length theory for turbulent eddy diffusion,

$$\frac{\partial}{\partial z} \int_0^b 2r\overline{w^2} dr \approx -\frac{\kappa}{2\alpha} b^2 \frac{\partial}{\partial z} \left[bW \frac{\partial W}{\partial z} \right], \tag{3.1}$$

where $\kappa > 0$ is a dimensionless parameter characterizing the diffusion of momentum through the action of turbulent eddies whose length scale is set by the radius of the plume. The equation expressing the balance of axial momentum proposed by Scase & Hewitt (2012) is then given by

$$\frac{\partial Q}{\partial t} + S \frac{\partial M}{\partial z} = \frac{QF}{M} + \frac{\kappa}{2\alpha} \frac{Q^2}{M} \frac{\partial}{\partial z} \left[\sqrt{M} \frac{\partial}{\partial z} \left(\frac{M}{Q} \right) \right]. \tag{3.2}$$

Scase & Hewitt (2012) provide numerical evidence that the diffusive term leads to a well-posed system of equations. It should be noted that, while Scase & Hewitt (2012) take $S \equiv 1$, in the analysis presented below we analyse the more general problem of $S \geq 1$.

Scase & Hewitt (2012) show that steady power-law solutions for pure-plume boundary conditions exist for the diffusive system (with $\kappa > 0$ anticipated to be small), and the structural change to the system of equations leads to a small modification of the solutions of Morton *et al.* (1956) (given by (2.13) with $S = 1$). The steady solutions of the ‘regularized’ system of equations with turbulent diffusion of momentum are given by (Scase & Hewitt 2012)

$$Q_0^{(SH)} = q_0 \left(1 - \frac{\kappa}{10S} \right)^{-1/3} z^{5/3}, \tag{3.3a}$$

$$M_0^{(SH)} = m_0 \left(1 - \frac{\kappa}{10S} \right)^{-2/3} z^{4/3}, \tag{3.3b}$$

$$F_0^{(SH)} = F_0. \tag{3.3c}$$

However, we find that these power-law solutions are spatially unstable. Indeed, taking perturbations of the form

$$Q^{(SH)}(z) = Q_0^{(SH)}(z)(1 + \epsilon Q_1^{(SH)}(z)), \quad M^{(SH)}(z) = M_0^{(SH)}(z)(1 + \epsilon M_1^{(SH)}(z)) \tag{3.4a,b}$$

(noting that the buoyancy flux $F(z) \equiv F_0$ for a plume in an unstratified ambient), where $\epsilon > 0$ is an ordering parameter, and linearizing the governing ordinary differential equations (for $\epsilon \ll 1$), we obtain

$$z \frac{dQ_1^{(SH)}}{dz} + \frac{5}{3} Q_1^{(SH)} - \frac{5}{6} M_1^{(SH)} = 0, \tag{3.5a}$$

$$\begin{aligned} \frac{6\kappa}{5S} z^2 \left(\frac{d^2 M_1^{(SH)}}{dz^2} - \frac{d^2 Q_1^{(SH)}}{dz^2} \right) - 2 \left(1 + \frac{\kappa}{10S} \right) z \frac{dM_1^{(SH)}}{dz} \\ + \frac{8}{3} Q_1^{(SH)} + 4 \left(\frac{\kappa}{10S} - \frac{4}{3} \right) M_1^{(SH)} = 0. \end{aligned} \tag{3.5b}$$

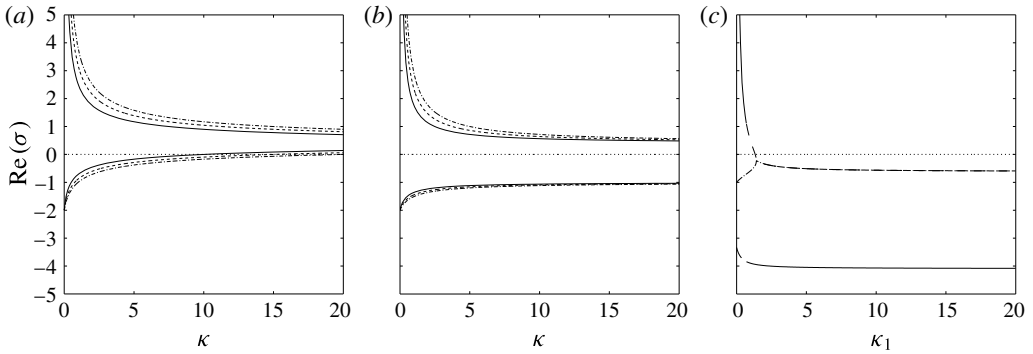


FIGURE 1. Spatial growth rates $\text{Re}(\sigma)$ as a function of the diffusion coefficient for (a) the Scase & Hewitt (2012) system with momentum diffusion (3.2), (b) the alternative form of the momentum diffusion equation (3.8) and (c) diffusion of buoyancy (3.11). In (a,b) different values of the momentum shape factor are shown, with $S=1$ (solid line), $S=1.5$ (dashed line) and $S=2$ (dash-dot line). In (c) the three branches of the growth rates are distinguished, with one branch corresponding to a real mode (solid line) and two branches that form a complex conjugate pair (dashed and dash-dot lines).

Seeking solutions of the form $Q_1^{(SH)} = q_1 z^\sigma$ and $M_1^{(SH)} = m_1 z^\sigma$, we find that non-trivial solutions are possible if $\sigma = \sigma_1 = -1$ or

$$\sigma = \sigma_{\pm} = \frac{5S + 4\kappa \pm \sqrt{25S^2 + 240S\kappa - 4\kappa^2}}{6\kappa}. \quad (3.6)$$

At least one of $\sigma_{\pm} > 0$ for $\kappa > 0$ for any $S \geq 1$ (figure 1a) and therefore the steady solutions of the Scase & Hewitt (2012) ‘regularized’ model are potentially spatially unstable. The growing modes can be suppressed by the application of a boundary condition on a truncated domain (Scase & Hewitt 2012), but we note that the system of equations for an unstratified ambient is formally applied on a semi-infinite domain without a far-field boundary condition. We note that, in the limit $\kappa = 0$, we find that σ_+ no longer appears in the analysis, while $\sigma_- \rightarrow -10/3$, and therefore the steady solutions become spatially stable (as expected, since the ‘regularized’ system reduces to the classical Morton *et al.* (1956) plume model). Spatial instability of the steady solutions is also found in a stratified ambient (not shown here), and in this case leads to severe difficulties as steady solutions cannot, in general, be found analytically, and the spatial instability precludes the numerical computation of steady solutions. Therefore, while the diffusive term introduced by Scase & Hewitt (2012) into the momentum balance resolves the ill-posedness in the unsteady plume model, the modification of the governing equations renders the steady solutions spatially unstable. While our present analysis considers pure-plume boundary conditions (i.e. $Q(0) = 0$, $M(0) = 0$ and $F(0) = F_0$), in appendix B we show that spatially stable steady solutions with arbitrary source conditions are not possible.

An alternative (although similar) form of the diffusion term can be formed by re-ordering the cross-sectional integration following the mixing-length parameterization of the fluctuation vertical momentum flux (with boundary terms introduced that are assumed small and subsequently neglected), so that we write

$$\frac{\partial}{\partial z} \int_0^b 2r\overline{w^2} dr \approx -\frac{\kappa}{2\alpha} \frac{\partial}{\partial z} \left[b^3 W \frac{\partial W}{\partial z} \right], \quad (3.7)$$

in place of (3.1). We then obtain the following expression for conservation of momentum:

$$\frac{\partial Q}{\partial t} + S \frac{\partial M}{\partial z} = \frac{QF}{M} + \frac{\kappa}{2\alpha} \frac{\partial}{\partial z} \left[\frac{Q^2}{\sqrt{M}} \frac{\partial}{\partial z} \left(\frac{M}{Q} \right) \right]. \tag{3.8}$$

The corresponding steady solutions are

$$Q_0^{(SH2)} = q_0 \left(1 + \frac{\kappa}{5S} \right)^{-1/3} z^{5/3}, \tag{3.9a}$$

$$M_0^{(SH2)} = m_0 \left(1 + \frac{\kappa}{5S} \right)^{-2/3} z^{4/3}, \tag{3.9b}$$

$$F_0^{(SH2)} = F_0, \tag{3.9c}$$

and a spatial stability analysis gives growth rates $\sigma = \sigma_{\pm} = -1$ or

$$\sigma = \sigma_{\pm} = \frac{5S - 3\kappa \pm \sqrt{25S^2 + 170S\kappa + 49\kappa^2}}{10\kappa}. \tag{3.10}$$

Thus, as with the Scase & Hewitt (2012) momentum diffusion term, there is a growing mode (figure 1b), and the steady solutions are spatially unstable.

Finally, we consider the change to the classical steady solutions of Morton *et al.* (1956) that occurs when a diffusive term is included in the equation for conservation of buoyancy (2.10c) rather than in the equation for conservation of momentum (i.e. we now take $\kappa = 0$). We again appeal to the Prandtl mixing-length theory to model the fluctuation of the flux of buoyancy, and obtain the following diffusive equation for the conservation of buoyancy:

$$\frac{\partial}{\partial t} \left(\frac{QF}{M} \right) + \frac{\partial F}{\partial z} = \frac{\kappa_1}{2\alpha} \frac{\partial}{\partial z} \left[\frac{Q^2}{\sqrt{M}} \frac{\partial}{\partial z} \left(\frac{F}{Q} \right) \right], \tag{3.11}$$

where κ_1 is a dimensionless parameter that describes the strength of the diffusion of buoyancy. The classical steady solutions (2.13) for pure-plume boundary conditions remain as solutions of the system (and other possible solutions cannot satisfy the pure-plume boundary condition at $z = 0$). However, a spatial stability analysis of the steady solutions (here including perturbations to the buoyancy flux in addition to the mass and momentum fluxes) shows that small-amplitude perturbations to the steady solutions are amplified unless the magnitude of the turbulence-induced diffusion is relatively large ($\kappa_1 > 4/3$, figure 1c).

The consequences of these analyses are that, while axial diffusivity effects may capture some important unsteady processes in the mixing of momentum or buoyancy, the form of the parameterization significantly alters the steady states attainable by the system. Indeed, the states equivalent to those established by Morton *et al.* (1956) have become spatially unstable, and therefore the unsteady model with axial diffusivity is not able to describe the steady states without an *ad hoc* far-field boundary condition.

4. Well-posedness of the hyperbolic unsteady plume model

As the turbulent diffusive terms, modelled phenomenologically using a Prandtl mixing-length approach, lead to a pathology in the integral plume model whereby the well-established steady states of Morton *et al.* (1956) cannot be obtained, the regularization through eddy diffusion, while potentially physically appealing, is

mathematically problematic. We therefore seek an alternative regularization of the system of unsteady integral equations; specifically, we examine the non-diffusive system of equations (i.e. we neglect the turbulent diffusive terms in (2.10), as suggested by Morton 1971) but allow the momentum shape factor to differ from unity to describe the different rates of transport of mass and momentum that result from non-uniform radial profiles. Thus, from here on in we study the non-diffusive system of equations

$$\frac{\partial}{\partial t} \left(\frac{Q^2}{M} \right) + \frac{\partial Q}{\partial z} = 2\alpha\sqrt{M}, \quad \frac{\partial Q}{\partial t} + S \frac{\partial M}{\partial z} = \frac{QF}{M}, \quad \frac{\partial}{\partial t} \left(\frac{QF}{M} \right) + \frac{\partial F}{\partial z} = 0. \tag{4.1a-c}$$

The system (4.1) is strictly hyperbolic when $S > 1$, with three real characteristic wave speeds given by

$$c_0 = M/Q \quad \text{and} \quad c_{\pm} = (S \pm \sqrt{S(S-1)})M/Q. \tag{4.2a,b}$$

We note, however, that in the limit $S \rightarrow 1$ there is a loss of hyperbolicity since the eigenvectors of the characteristic equation for the system (4.1) do not span \mathbb{R}^3 , although the wave speeds remain real and equal to c_0 ; the system is formally parabolic for $S = 1$ (Scase *et al.* 2006b). As we demonstrate below, the change in the characteristic structure, and so change in type, of the governing equations that occurs for $S = 1$ fundamentally alters solutions of the system of equations. (It should be noted that if a shape factor for the buoyancy flux that differs from unity is included in (4.1c), then $c_0 = S_f M/Q$ while c_{\pm} remain unchanged, and a loss of hyperbolicity occurs if $S_f = S \pm \sqrt{S(S-1)}$.)

In order to establish well-posedness of the system of equations, we analyse the evolution of small perturbations to the steady solutions. It is convenient for subsequent analysis and numerical computations to factor out the steady solution and to introduce a new spatial coordinate, $x = (q_0/m_0)z^{4/3}$. We consider the stability of the steady solution to small perturbations. Therefore, we introduce an ordering parameter $\epsilon \ll 1$ and perturbations to the steady solution of the form

$$Q(x, t) = Q_0(x)(1 + \epsilon q(x, t)), \tag{4.3a}$$

$$M(x, t) = M_0(x)(1 + \epsilon m(x, t)), \tag{4.3b}$$

$$F(x, t) = F_0(1 + \epsilon f(x, t)), \tag{4.3c}$$

and linearize the governing equation (4.1) to obtain

$$\mathbf{A} \frac{\partial \mathbf{q}}{\partial t} + \frac{4}{3} \mathbf{B} \frac{\partial \mathbf{q}}{\partial x} + \mathbf{C} \frac{1}{x} \mathbf{q} = \mathbf{0}, \tag{4.4}$$

where $\mathbf{q} = (q, m, f)^T$ and the matrices \mathbf{A} , \mathbf{B} and \mathbf{C} are given by

$$\mathbf{A} = \begin{pmatrix} 2 & -1 & 0 \\ 1 & 0 & 0 \\ 1 & -1 & 1 \end{pmatrix}, \quad \mathbf{B} = \begin{pmatrix} 1 & 0 & 0 \\ 0 & S & 0 \\ 0 & 0 & 1 \end{pmatrix} \quad \text{and} \quad \mathbf{C} = \begin{pmatrix} 5/3 & -5/6 & 0 \\ -4S/3 & 8S/3 & -4S/3 \\ 0 & 0 & 0 \end{pmatrix}. \tag{4.5a-c}$$

When $S \equiv 1$ the system (4.1) was shown to be ill-posed by Scase & Hewitt (2012), who examined the response of the linearized system of equations to small-amplitude harmonic variation of frequency ω in the source buoyancy flux, and found a closed

form solution for the perturbations in terms of special functions. It was shown that the amplitude of the perturbations grows with the distance from the source as $\omega^{-7/8}x^{-7/8} \exp(\sqrt{15\omega x}/4)$ for $x \gg 1$ (Scase & Hewitt 2012). Thus, the steady solutions are linearly unstable, as the amplitudes of the perturbations grow as they propagate away from the source, and, furthermore, the system of equations (4.1) with $S = 1$ is ill-posed since high-frequency fluctuations increase in amplitude most rapidly with no cutoff (Scase & Hewitt 2012).

For $S > 1$ we are unable to find closed form solutions of the linear system (4.4). We therefore examine the evolution of perturbations in the far field through an asymptotic analysis of the linear system (4.4) in the neighbourhood of the irregular singular point $x \rightarrow \infty$ (Bender & Orszag 1978). We consider two stability problems: an initial-value problem where the evolution of an arbitrary initial perturbation \mathbf{q} with compact support

$$\mathbf{q}(x, 0) = \mathbf{q}_0(x) \quad \text{with } \mathbf{q}_0(x) \rightarrow 0 \text{ as } x \rightarrow \infty \tag{4.6}$$

is investigated, and a boundary-value problem where a fluctuation at the source $x = 0$ is imposed and the response of the system downstream of the source is examined. Both of these problems can be analysed conveniently through the use of integral transforms of the linear system (4.4); a Laplace transform in time for the initial-value problem and a Fourier transform in time for the boundary-value problem. Denoting the Laplace transform of $\mathbf{q}(x, t)$ as $\hat{\mathbf{q}}(x, p)$ (with the Fourier transform obtained by taking $p = i\omega$, where ω is the frequency of the harmonic source fluctuation imposed in the boundary-value problem), we obtain

$$p\mathbf{A}\hat{\mathbf{q}} + \frac{4}{3}\mathbf{B}\frac{d\hat{\mathbf{q}}}{dx} + \frac{1}{x}\mathbf{C}\hat{\mathbf{q}} = \mathbf{A}\mathbf{q}_0. \tag{4.7}$$

The far-field behaviour is obtained conveniently by letting $\hat{\mathbf{q}} = \mathbf{f}(x)e^{g(x)}$ (Bender & Orszag 1978), with $g(x)$ a singular function and $\mathbf{f}(x)$ regular as $x \rightarrow \infty$, so $\mathbf{f}(x) = \mathbf{f}_0 + \mathbf{f}_1x^{-1} + \mathbf{f}_2x^{-2} + \dots$ for $x \gg 1$. The linear system (4.7) can then be written as

$$\frac{4}{3}\mathbf{B}\frac{d\mathbf{f}}{dx} + \left(p\mathbf{A} + \frac{4}{3}\mathbf{B}\frac{dg}{dx} + \frac{1}{x}\mathbf{C} \right) \mathbf{f} = 0. \tag{4.8}$$

A leading-order balance requires $g(x) \sim p\lambda x$ as $x \rightarrow \infty$. Then λ and \mathbf{f}_0 satisfy the generalized eigenproblem $\mathbf{A}\mathbf{f}_0 = -4\lambda\mathbf{B}\mathbf{f}_0/3$, and therefore

$$\lambda = \lambda_0 = -\frac{3}{4}, \quad \text{with } \mathbf{f}_0 = \mathbf{f}_{00} = (0, 0, 1)^T, \quad \mathbf{f}_0^L = \mathbf{f}_{00}^L = (-1, 0, 1), \tag{4.9a}$$

$$\lambda = \lambda_+ = -\frac{3}{4} \left(\frac{S + \sqrt{S(S-1)}}{S} \right), \quad \text{with } \mathbf{f}_0 = \mathbf{f}_{0+} = \left(1, \frac{1 - (S - \sqrt{S(S-1)})}{\sqrt{S(S-1)}}, 1 \right)^T, \\ \mathbf{f}_0^L = \mathbf{f}_{0+}^L = (S + \sqrt{S(S-1)}, -1, 0), \tag{4.9b}$$

$$\lambda = \lambda_- = -\frac{3}{4} \left(\frac{S - \sqrt{S(S-1)}}{S} \right), \quad \text{with } \mathbf{f}_0 = \mathbf{f}_{0-} = \left(1, -\frac{1 - (S + \sqrt{S(S-1)})}{\sqrt{S(S-1)}}, 1 \right)^T, \\ \mathbf{f}_0^L = \mathbf{f}_{0-}^L = (S - \sqrt{S(S-1)}, -1, 0), \tag{4.9c}$$

where \mathbf{f}_0^L denotes the left eigenvector satisfying $\mathbf{f}_0^L\mathbf{A} = -4\lambda\mathbf{f}_0^L\mathbf{B}/3$.

To proceed further we let $g(x) \sim p\lambda x + \mu \log x$ for $x \gg 1$. Substitution into (4.8) and balancing coefficients of x gives, at order $O(1/x)$,

$$p(\mathbf{A} + \frac{4}{3}\lambda\mathbf{B})\mathbf{f}_1 + (\frac{4}{3}\mu\mathbf{B} + \mathbf{C})\mathbf{f}_0 = \mathbf{0}, \tag{4.10}$$

and so, by multiplying on the left by \mathbf{f}_0^L , we find

$$\mu = -\frac{3\mathbf{f}_0^L\mathbf{C}\mathbf{f}_0}{4\mathbf{f}_0^L\mathbf{B}\mathbf{f}_0}, \tag{4.11}$$

and therefore

$$\mu = \mu_0 = 0 \quad \text{when } \lambda = \lambda_0, \tag{4.12a}$$

$$\mu = \mu_+ = -\frac{13}{8} - \frac{5(2S-1)}{16\sqrt{S(S-1)}} \quad \text{when } \lambda = \lambda_+, \tag{4.12b}$$

$$\mu = \mu_- = -\frac{13}{8} + \frac{5(2S-1)}{16\sqrt{S(S-1)}} \quad \text{when } \lambda = \lambda_+. \tag{4.12c}$$

The coefficient vectors ($\mathbf{f}_1, \mathbf{f}_2$, etc.) can be determined from higher-order terms in the expansion but are not given here.

The leading-order behaviour in the far field is therefore given by

$$\mathbf{q}(x, t) \sim \mathbf{f}_0 x^\mu \delta(t - \lambda x), \tag{4.13}$$

where $\delta(x)$ denotes the Dirac delta function, corresponding to the propagation of discontinuities whose strength varies algebraically with distance from the source. The amplitude of the perturbations grows if $1 < S < 25/24$, whereas the amplitude decays algebraically if $S > 25/24$, as shown in figure 2. Importantly, the algebraic growth rates μ do not depend on the transform variable p . Therefore, for the initial-value problem the evolution of perturbations in the far field is independent of the spatial length scale of the initial perturbation, whereas when considering a boundary-value problem the growth rate of the perturbations does not depend on the frequency of the harmonic boundary oscillations. Therefore, the far-field asymptotic analysis shows that the system (4.1) with $S > 1$ is well-posed as there is a continuous dependence of the solutions on the initial or boundary data, and small scales (either spatial scales in the case of an initial-value problem or temporal scales for a boundary-value problem) are not amplified more rapidly than longer scales. This is in contrast to the far-field limit of the solution of a boundary-value problem that is determined by Scase & Hewitt (2012), where exponential growth of the amplitude of perturbations is found with a growth rate that increases exponentially with $\sqrt{\omega}$, and therefore when $S = 1$ the system of equations is ill-posed. The distinguished behaviour for $S = 1$ is apparent in the eigenvectors \mathbf{f}_{0+} and \mathbf{f}_{0-} , which are singular in the limit $S \rightarrow 1$. Numerical solutions demonstrating the evolution of a localized initial perturbation are presented in § 5.

5. Solutions of the well-posed unsteady plume model

We consider now solutions of the nonlinear system of equations (4.1) with $S > 1$. As the system of equations (4.1) is hyperbolic in this parameter regime, solutions may exhibit discontinuities, across which we enforce the following jump conditions that

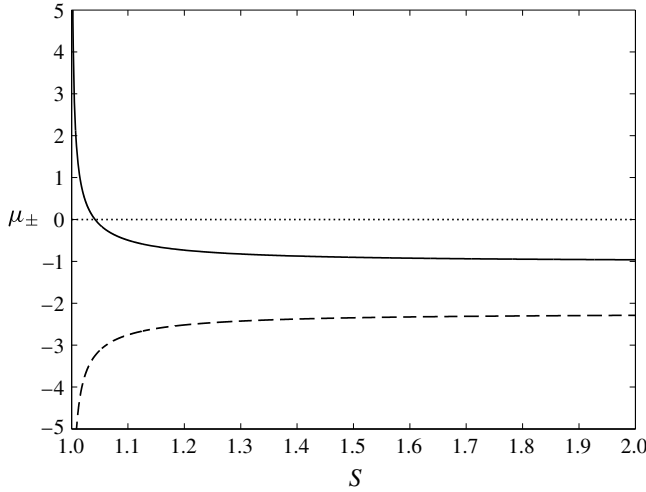


FIGURE 2. The exponents of the far-field algebraic growth rates of the amplitude of the volume flux perturbation, μ_+ (dashed line) and μ_- (solid line), as functions of the shape factor S . The perturbation to the volume flux grows with increasing distance from the source when $\mu_- > 0$, which occurs for $S < 25/24$.

respectively impose the conservation of mass, momentum and buoyancy fluxes over a discontinuity at $z = z_s(t)$, moving with velocity $c = dz_s/dt$,

$$\left[Q - c \frac{Q^2}{M} \right]_{z=z_s^-}^{z=z_s^+} = 0, \quad [SM - cQ]_{z=z_s^-}^{z=z_s^+} = 0 \quad \text{and} \quad \left[F - c \frac{QF}{M} \right]_{z=z_s^-}^{z=z_s^+} = 0. \quad (5.1a-c)$$

These jump conditions admit two different types of discontinuous solutions, which are more easily analysed in terms of the primitive variables b , W and G' . Further denoting the values of the dependent variables either side of the discontinuity with superscripts $+$ and $-$, corresponding to $z = z_s^+$ and $z = z_s^-$ respectively, we find that provided the velocity is discontinuous ($W^+ \neq W^-$) then the reduced gravity G' is continuous (i.e. $G'^+ = G'^-$). Furthermore, in this case, by eliminating b^+ and b^- , we find that

$$(W^+ - W^-)(c^2 - cS(W^+ + W^-) + SW^+W^-) = 0. \quad (5.2)$$

When the shape factor is equal to unity, the only solution is $c = W^+ = W^-$, and this contradicts the assumption that there is a discontinuity. Thus, for $S = 1$ it is not possible to construct discontinuous solutions. However, when $S > 1$, we find

$$c = \frac{1}{2}S(W^+ + W^-) - \frac{1}{2}(S^2(W^+ + W^-)^2 - 4SW^+W^-)^{1/2}, \quad (5.3)$$

where the negative root has been chosen so that $W^- > c$, a condition required for causality. The other type of discontinuity occurs when $W^+ = W^- = c$. Then the radius of the plume is also continuous, $b^+ = b^-$, but the reduced gravity may be discontinuous and potentially even unbounded. We refer to this latter form as a ‘contact’ discontinuity, which occurs due to a linearly degenerate field in the system of equations (Lax 1973).

To calculate numerically solutions of the nonlinear hyperbolic system of equations, we employ the non-oscillatory central scheme of Kurganov & Tadmor (2000) with

a third-order total variation diminishing Runge–Kutta time stepping scheme (Gottlieb & Shu 1998), using an adaptive time step that ensures that the Courant–Friedrichs–Lewy (CFL) number remains fixed at 1/8 to maintain numerical stability. The high-resolution central scheme is a shock-capturing numerical method for conservation laws (Kurganov & Tadmor 2000) and has been used extensively to compute solutions of nonlinear hyperbolic systems. For numerical convenience, we factor out the steady solutions from the dependent variables and compute solutions in the transformed spatial coordinate x as, although the system is not autonomous in this representation, the characteristic wave speeds remain bounded near to the source (i.e. as $x \rightarrow 0$) when the steady solution is realized, whereas the wave speeds of the system (4.1) diverge as $z \rightarrow 0$. Therefore, in the mapped variables, we can take larger time steps while maintaining numerical stability.

We consider first the evolution of a perturbation to the steady solution (2.13) to confirm the far-field asymptotic analysis in §4. We take as an initial condition a Gaussian perturbation (in the transformed coordinate x) to the steady momentum flux of the form

$$M(x, 0)/M_0(x) = 1 + 0.01e^{-10(x-5)^2}, \quad (5.4)$$

while the volume flux and buoyancy flux are not perturbed from the steady values, and take the shape factor to be $S = 1.1$ ($> 25/24$). We compute numerically the evolution of the perturbation using the Kurganov & Tadmor (2000) central scheme for the nonlinear system rather than using the linearized equations, since the linearization introduces a subtle structural change in the governing equations: for the linearized system, all fields are (trivially) linearly degenerate and so discontinuities are of the contact discontinuity type (Lax 1973), whereas two fields in the nonlinear system are genuinely nonlinear. We find that the Kurganov & Tadmor (2000) scheme resolves the shocks and rarefactions associated with the genuinely nonlinear fields accurately, but has less accuracy when contact discontinuities occur for linearly degenerate fields (see, e.g., Kurganov & Petrova 2000). In order to track the evolution of the perturbations to long times (and so large distance from the source), we implement a moving numerical domain, using the characteristic wave speeds of the linearized system to advect the lower and upper grid points, with boundary conditions in the moving domain given by the respective steady states. The numerical domain is then advected downstream, and the number of grid points increases as the spatial extent of the perturbation grows in order to maintain a specified numerical resolution.

In figure 3 we illustrate the evolution of the initial perturbation for dimensionless times $t \leq 40$ (noting that, for pure-plume source conditions, the time scale of motion, τ , is related to the length scale, Z , and the source buoyancy flux, F_0 , through $\tau = Z^{4/3}F_0^{-1/3}$), showing the perturbations to the plume radius, mass flux and buoyancy flux as functions of the scaled spatial coordinate x . The initial perturbation develops into a pulse whose spatial extent grows as it propagates. The amplitude of the perturbation slowly decreases, demonstrating linear stability of the system of equations for $S = 1.1$. The three discontinuities are apparent in the evolving perturbation, with the contact discontinuity that propagates at the speed of the intermediate characteristic most clearly seen in the perturbation to the reduced gravity, G' .

We introduce integral measures of the amplitude of the perturbations, with

$$\mathcal{I}(Q) = \int_0^\infty \left(\frac{Q(x, t)}{Q_0(x)} - 1 \right)^2 dx \quad (5.5)$$

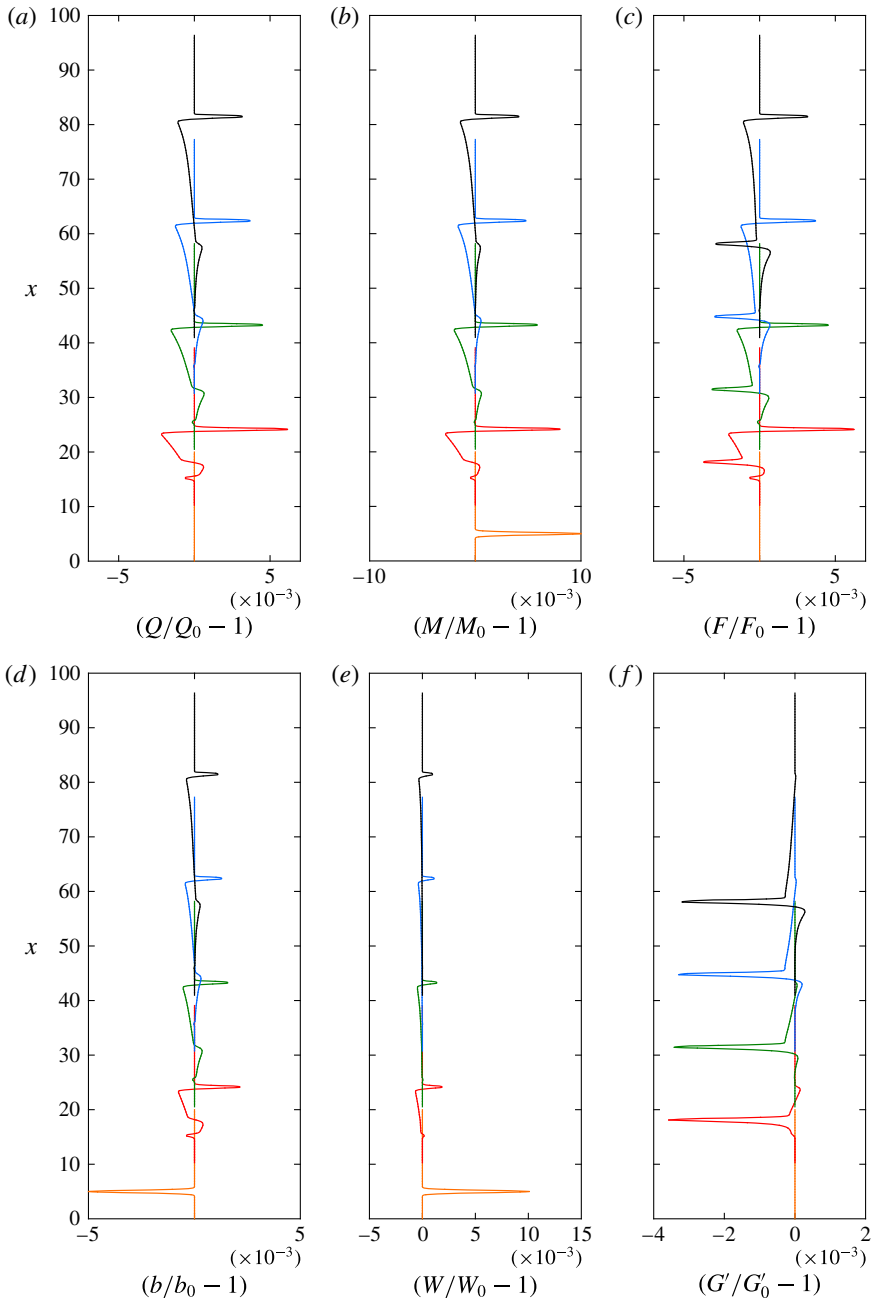


FIGURE 3. (Colour online) The perturbations to the fluxes of volume, $Q/Q_0 - 1$ (a), momentum, $M/M_0 - 1$ (b), and buoyancy, $F/F_0 - 1$ (c), and to the plume radius, $b/b_0 - 1$ (d), the plume velocity, $W/W_0 - 1$ (e), and the reduced gravity, $G'/G'_0 - 1$ (f), as functions of the scaled distance from the source, x , for dimensionless times $t=0$ (orange), $t=10$ (red), $t=20$ (green), $t=30$ (blue), and $t=40$ (black). The momentum shape factor is fixed at a value $S = 1.1 > 25/24$. The numerical solution scheme adopts a moving and expanding spatial grid with a fixed grid spacing of $\Delta x = 0.01$.

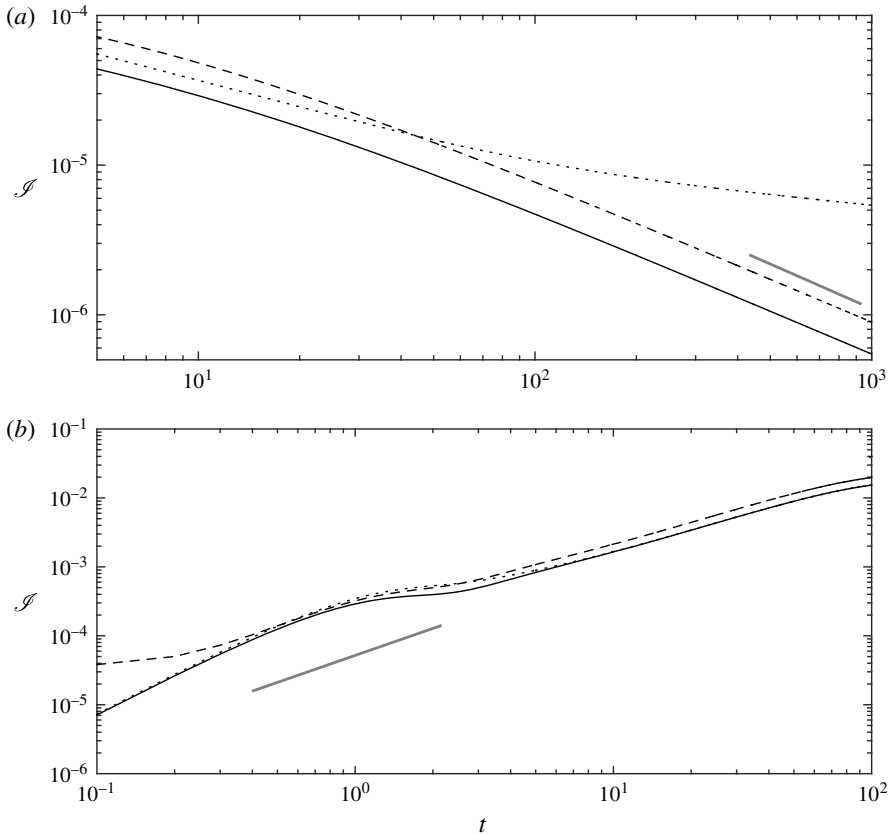


FIGURE 4. Integral measures of the size of perturbations from the steady solutions for the volume flux, $\mathcal{I}(Q)$ (solid line), momentum flux, $\mathcal{I}(M)$ (dashed line), and buoyancy flux, $\mathcal{I}(F)$ (dotted line), as functions of the dimensionless time t , for a shape factor (a) $S = 1.1 > 25/24$ and (b) $S = 1.02 < 25/24$. The thick grey line illustrates the predicted growth rate of perturbations of $t^{2\mu_+}$ with (a) $\mu_+ \approx -0.49$ for $S = 1.1$ and (b) $\mu_+ \approx 0.65$ for $S = 1.02$ obtained from the far-field asymptotic analysis (4.12b).

for the volume flux, and similarly for the fluxes of momentum and buoyancy. Figure 4(a) shows the time evolution of $\mathcal{I}(Q)$, $\mathcal{I}(M)$ and $\mathcal{I}(F)$ when the shape factor $S = 1.1$. Following a short transient reorganization of the initial condition for $t < 5$ (not shown in the figure), the perturbations to the steady solution decay as they propagate through the domain. The perturbations to the steady fluxes of volume and momentum closely follow the prediction of the far-field analysis for $t > 100$, at which time the signal of the perturbation that travels with the fastest characteristic has reached $x \approx 197$. The decay in the perturbation to the buoyancy flux is less rapid, and the rate of decay diminishes as time progresses. This is expected from the far-field asymptotic analysis of the linearized system, where a component of the buoyancy flux is found to be advected at the speed of the plume without change in amplitude (see (4.12a)).

For $1 < S < 25/24$ our far-field asymptotic analysis shows that the steady solutions are linearly unstable. Numerical solutions of the governing equations support the asymptotic analysis, as illustrated in figure 4(b), which shows the time evolution of

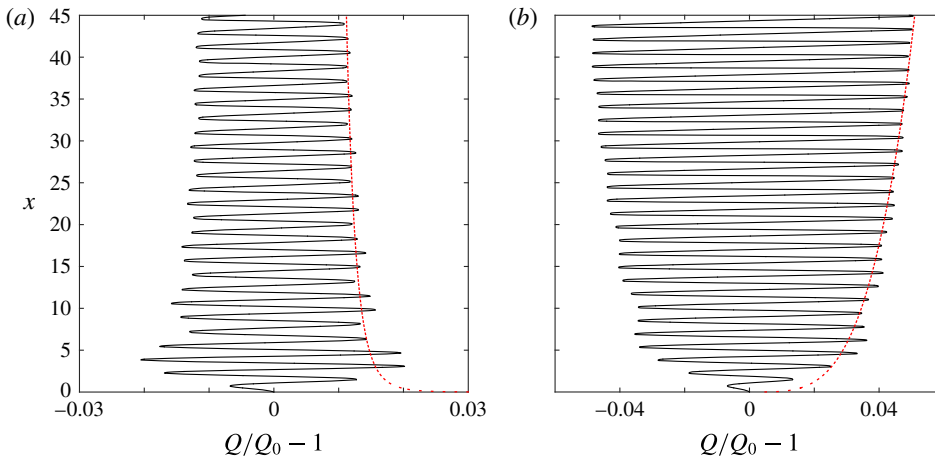


FIGURE 5. (Colour online) The perturbation to the steady volume flux due to harmonic oscillation of the source buoyancy flux with period 2π as a function of the scaled spatial coordinate x at dimensionless time $t = 99$ for a shape factor of (a) $S = 1.05 > 25/24$ and (b) $S = 1.03 < 25/24$. The red dashed line illustrates an algebraic growth of perturbations of the form cx^μ , where (a) $\mu = -0.12$ for $S = 1.05$ and (b) $\mu = 0.26$ for $S = 1.03$. The prefactor c is selected to provide an envelope of the numerical solution.

the integral measures of the size of the perturbations for a shape factor $S = 1.02$ ($< 25/24$). For early times ($t < 10$) the perturbations to the steady solutions grow algebraically with a growth rate that is close to the growth rate predicted from the far-field analysis. We note that at early times the perturbation has not propagated far downstream from the localized initial condition and therefore the far-field asymptotic analysis would not be expected to describe fully the evolution. At later times ($t > 50$) the growth of the perturbations deviates substantially from the predictions of the linear far-field analysis as nonlinear effects begin to influence the evolution.

Numerical solutions of the governing equations also support the far-field asymptotic analysis of the linearized system when a harmonic oscillation of the source boundary conditions is imposed. Figure 5 illustrates the spatial structure of the perturbation to the steady volume flux at time $t = 99$ for a shape factor of $S = 1.05 > 25/24$ (figure 5a) and $S = 1.03 < 25/24$ (figure 5b). The far-field analysis predicts linear stability when $S = 1.05$ and instability when $S = 1.03$, and this is observed in the numerical solutions, with the amplitude of perturbations decaying with increasing distance downstream when $S = 1.05$ (figure 5a), in contrast to the growth in the amplitude of the perturbations that is seen when $S = 1.03$ (figure 5b).

6. Similarity solutions for the unsteady evolution of plumes following an abrupt change in the source buoyancy flux

We examine now the nonlinear evolution of plumes following an abrupt change in the source conditions. Specifically, we consider solutions of the system of nonlinear evolution equations (4.1) with $S > 25/24$ (so that the steady states are linearly stable) for an initial boundary-value problem in which the magnitude of the buoyancy flux at the source is instantaneously changed from F_0 to F_1 at $t = 0$. For $t < 0$ the plume is in a steady state given by (2.13) and (2.14). We calculate the unsteady evolution as the plume adjusts to the new steady state in which the buoyancy flux, F_0 , in (2.13) and

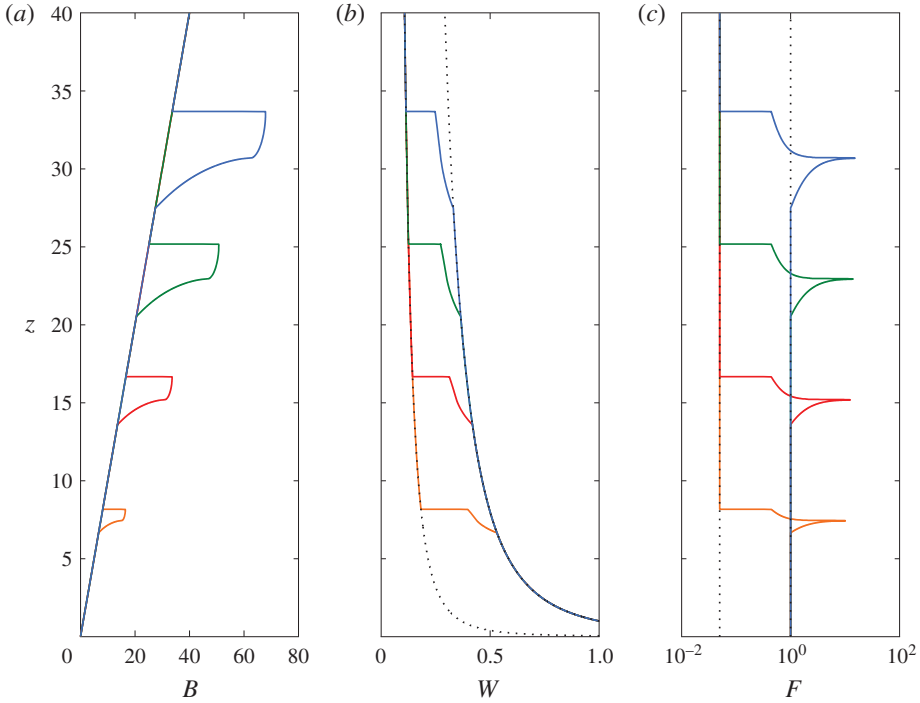


FIGURE 6. (Colour online) The scaled width, $B(z) = z\widehat{Q}/\widehat{M}^{1/2}$, the scaled velocity, $W(z) = z^{-1/3}\widehat{M}/\widehat{Q}$, and the buoyancy flux, \widehat{F} , as functions of the distance from source, z at dimensionless times $t = 2.4$ (orange), $t = 4.9$ (red), $t = 7.4$ (green) and $t = 9.9$ (blue) for an increase in buoyancy flux ($\mathcal{F} = 0.05$) at $t = 0$ and with shape factor $S = 1.1$. In (b) the scaled velocity $W = z^{-1/3}$, corresponding to the steady velocity field of the original buoyancy flux at the source, and the scaled velocity $W = z^{-1/3}20^{1/3}$, corresponding to the steady velocity field associated with the new buoyancy flux, are plotted with dashed lines. In (c) the original buoyancy flux, $F = F_0 = 0.05$, and the new steady-state buoyancy flux, $F = F_1 = 1$, are plotted with dashed lines.

(2.14) is replaced by F_1 . Thus, the initial conditions are given by (2.13) and (2.14), while for $t > 0$ the new source conditions for the plume are given by $F(0, t) = F_1$ and $Q(0, t) = M(0, t) = 0$.

The numerical solutions demonstrate that the adjustment occurs by the advection of an unsteady ‘pulse’ through the environment (see figures 6, 8 and 10 for examples of computations), which is modelled by the nonlinear evolution equations (4.1). In this section we draw out the self-similar adjustment that occurs in the dependent variables.

The similarity variable is established through the following scaling analyses, which require all of the terms in the governing partial differential equations (4.1) to be of the same order. To this end, to balance all of the derivative terms we require $M \sim Qz/t$. Turning then to the ‘source’ terms, from (4.1a) we have $Q/z \sim M^{1/2}$, while from (4.1b) $M/z \sim QF_1/M$, where we have used $F \sim F_1$ as the scale of the buoyancy flux. Together these yield $z^4 \sim F_1 t^3$, and we therefore seek similarity solutions to the system in terms of this gearing between the spatial and temporal scales. We note that the existence of this similarity grouping was identified by Scase *et al.* (2006b) (see also Scase *et al.* 2008), although they did not construct the complete similarity

solution; indeed, for their system with $S = 1$ it was not possible to do so because the ill-posedness of the system is manifested as irreconcilable divergences in the solution (see § 4). Instead, Scase *et al.* (2006*b*) found a separable solution that did not satisfy the boundary conditions but did capture some of the features found in their numerical computation. We discuss in appendix C the counterpart to their separable solution in the now regularized system of governing equations. Before analysing the form of the similarity solutions, we note that there is another reason for anticipating the similarity scaling deduced above: the system is hyperbolic for $S > 1$, and all of the characteristics are proportional to $W = M/Q \propto F_1^{1/3} z^{-1/3}$. The characteristic curves are of the form $dz/dt \propto W$, thus also admitting the similarity scaling $z^4 \sim F_1 t^3$, and it is through the evolution of the characteristics that the system adjusts to its new state.

We now seek similarity solutions for the fluxes of volume, momentum and buoyancy, which we write in the following form:

$$Q = \frac{6\alpha}{5} \left(\frac{9\alpha}{10S}\right)^{1/3} F_1^{1/3} z^{5/3} \widehat{Q}(\eta), \quad M = \left(\frac{9\alpha}{10S}\right)^{2/3} F_1^{2/3} z^{4/3} \widehat{M}(\eta) \quad \text{and} \quad F = F_1 \widehat{F}(\eta), \tag{6.1a-c}$$

where the similarity variable is given by

$$\eta = \frac{6\alpha}{5} \left(\frac{10S}{9\alpha}\right)^{1/3} \frac{z^{4/3}}{F_1^{1/3} t} \tag{6.2}$$

and the similarity functions $\widehat{Q}(\eta)$, $\widehat{M}(\eta)$ and $\widehat{F}(\eta)$ are to be determined. In this form the steady state given by (2.13) corresponds to constant values of \widehat{Q} , \widehat{M} and \widehat{F} . It is convenient to further substitute $\widehat{Q} = \eta \widehat{q}$, $\widehat{M} = \eta^2 \widehat{m}$ and $\widehat{F} = \eta^3 \widehat{f}$ because this simplifies the governing equations, which are now given by

$$\begin{pmatrix} \frac{4}{3} - 2\frac{\widehat{q}}{\widehat{m}} & \frac{\widehat{q}^2}{\widehat{m}^2} & 0 \\ -1 & \frac{4}{3}S & 0 \\ -\frac{\widehat{f}}{\widehat{m}} & \frac{\widehat{f}\widehat{q}}{\widehat{m}^2} & \frac{4}{3} - \frac{\widehat{q}}{\widehat{m}} \end{pmatrix} \eta \frac{d}{d\eta} \begin{pmatrix} \widehat{q} \\ \widehat{m} \\ \widehat{f} \end{pmatrix} = \begin{pmatrix} \frac{5}{3}\widehat{m}^{1/2} - 3\widehat{q} \\ \frac{4}{3}\frac{S\widehat{f}\widehat{q}}{\widehat{m}} - 4S\widehat{m} + \widehat{q} \\ -4\widehat{f} + \frac{2\widehat{f}\widehat{q}}{\widehat{m}} \end{pmatrix}. \tag{6.3}$$

Symbolically, we write this coupled differential system as $\mathbf{D}\eta \, d\widehat{\mathbf{q}}/d\eta = \mathbf{b}$, noting that both the matrix \mathbf{D} and the vector \mathbf{b} are only functions of the dependent variables $\widehat{\mathbf{q}} = (\widehat{q}, \widehat{m}, \widehat{f})$. We note that the ‘separable’ similarity solutions derived by Scase *et al.* (2006*b*) correspond to $\widehat{\mathbf{q}} = (\widehat{q}, \widehat{m}, \widehat{f}) = \text{constant}$, and these are discussed in appendix C. For the motion driven by an abrupt change in the magnitude of the buoyancy flux at source, the vital parameter is the ratio of the initial to final buoyancy fluxes at the source given by $\mathcal{F} = F_0/F_1$. We note that the initial conditions correspond to

$$(\widehat{q}, \widehat{m}, \widehat{f}) = \left(\frac{\mathcal{F}^{1/3}}{\eta}, \frac{\mathcal{F}^{2/3}}{\eta^2}, \frac{\mathcal{F}}{\eta^3}\right). \tag{6.4}$$

In terms of the similarity functions, these are enforced in the far field ($\eta \rightarrow \infty$) and correspond to the region that is unaffected by the change of the buoyancy flux at the source. The source conditions demand that

$$(\widehat{q}, \widehat{m}, \widehat{f}) \rightarrow \left(\frac{1}{\eta}, \frac{1}{\eta^2}, \frac{1}{\eta^3}\right) \quad \text{as } \eta \rightarrow 0. \tag{6.5}$$

Constructing the similarity solutions then corresponds to integrating the governing system of ordinary differential equations (6.3), subject to these conditions.

The matrix **D** is singular when

$$\left(\frac{4}{3} - \frac{\widehat{q}}{\widehat{m}}\right) \left(\frac{16}{9} - \frac{8S}{3} \frac{\widehat{q}}{\widehat{m}} + \frac{\widehat{q}^2}{\widehat{m}^2}\right) = 0. \tag{6.6}$$

This corresponds to locations where $\widehat{q}/\widehat{m} = 4/3$ and $\widehat{q}/\widehat{m} = 4(S \pm \sqrt{S^2 - S})/3$. These are singular points of the governing system of equations and are of significance because the dependent variables may have discontinuous gradients at these locations. We show in appendix D how to derive the local behaviour close to the singular points; this is required to initiate numerical integration from these locations.

The similarity solutions may also feature discontinuous solutions, in which case we define the shock position, $z_s(t)$, scaled according to the similarity variables to be given by

$$z_s^{4/3} = \frac{5}{6\alpha} \left(\frac{9\alpha}{10S}\right)^{1/3} F_1^{1/3} t \eta_s, \tag{6.7}$$

where η_s is a constant. In this case of discontinuous solutions, the jump conditions relate the dependent variables at $\eta = \eta_s^+$ to those at $\eta = \eta_s^-$ and are given by

$$\left[\widehat{q} - \frac{3\widehat{q}^2}{4\widehat{m}}\right]_+^+ = 0, \quad \left[S\widehat{m} - \frac{3\widehat{q}}{4}\right]_+^+ = 0 \quad \text{and} \quad \left[f - \frac{3\widehat{q}f}{4\widehat{m}}\right]_+^+ = 0. \tag{6.8a-c}$$

Key locations in the similarity solutions are the points at which the dependent variables transition from the new steady state to an unsteady pulse and then from this unsteady pulse to the original steady state. The family of slowest moving characteristics associated with the new source is given by

$$\frac{dz}{dt} = \frac{M}{Q} (S - \sqrt{S(S-1)}) = \frac{z\widehat{m}}{t\widehat{q}} (S - \sqrt{S(S-1)}). \tag{6.9}$$

The transition between the steady and unsteady portions of the solution must occur at a singular point of **D** to permit the gradient of the solution to change discontinuously. Thus, in this case $\widehat{q}/\widehat{m} = 4(S - \sqrt{S(S-1)})/3$, and so we find that

$$\frac{dz}{dt} = \frac{3z}{4t}. \tag{6.10}$$

This implies that the transition point occurs at a constant value of the similarity variables, $\eta = \eta_{c1}$, given by

$$\eta_{c1} = \frac{4}{3} (S - \sqrt{S(S-1)}), \tag{6.11}$$

using the condition (6.5). Likewise, the family of fastest moving characteristics is given by

$$\frac{dz}{dt} = \frac{M}{Q} (S + \sqrt{S(S-1)}) = \frac{z\widehat{m}}{t\widehat{q}} (S + \sqrt{S(S-1)}), \tag{6.12}$$

and so the boundary between the unsteady pulse and the steady solution associated with the original buoyancy flux occurs at a constant value of the similarity variable, $\eta = \eta_{c2}$, given by

$$\eta_{c2} = \frac{4}{3} \mathcal{F}^{1/3} (S + \sqrt{S(S-1)}), \tag{6.13}$$

using the condition (6.4), provided that the motion is due to a decrease in the source strength ($\mathcal{F} > 1$). If the source strength increases then the characteristics associated with the new release overtake those due to the original source and, as we show below, the motion forms ‘shocks’.

6.1. Increase in buoyancy flux

These flows correspond to a new scaled buoyancy flux such that $\mathcal{F} < 1$. For $\eta < \eta_{c1}$ the similarity solution is given by

$$(\hat{q}, \hat{m}, \hat{f}) = \left(\frac{1}{\eta}, \frac{1}{\eta^2}, \frac{1}{\eta^3} \right), \tag{6.14}$$

where η_{c1} is given by (6.11) and corresponds to the slowest moving characteristics associated with the new buoyancy flux. The leading edge of the unsteady solution corresponds to a shock at $\eta = \eta_s$ such that, for $\eta > \eta_s$, the solution is given by the steady state associated with the original buoyancy flux given by (2.13).

Construction of the similarity solution then requires the computation of the solution for $\eta_{c1} < \eta < \eta_s$, where η_s is to be determined as part of that solution. We note that this domain includes a location where $\hat{q}/\hat{m} = 4/3$. Here, there is the potential for a contact discontinuity where the reduced gravity is discontinuous or even unbounded, but the volume and momentum fluxes are continuous. The numerical problem is therefore a boundary-value ordinary differential equation with an internal critical point, which we solve using a numerical shooting technique. Our method of solution proceeds as follows. First, we numerically integrate from $\eta = \eta_{c1}$ using the local series expansion given in appendix D. This expansion provides a solution local to the critical point and entails an undetermined constant, C_σ . Given a value of C_σ , the numerical integration can be continued until $\eta = \eta_{m1}$, at which $\hat{q}/\hat{m} = 4/3$. The solution is also numerically integrated from the shock at the leading edge. Given a shock location η_s , the jump conditions (6.8) provide the conditions at $\eta = \eta_s^-$ and then the solutions may be numerically integrated until $\eta = \eta_{m2}$ at which $\hat{q}/\hat{m} = 4/3$. The constant C_σ and the shock location η_s are then iteratively adjusted until $\eta_{m1} = \eta_{m2}$ and $\hat{q}(\eta_{m1}) = \hat{q}(\eta_{m2})$ (noting that this ensures that the momentum flux is continuous at this location as well), and when these conditions are satisfied, this provides the entire solution.

The numerical integration of the governing partial differential equations is plotted in figure 6 at various instances of time, and the underlying similarity form of solution is plotted in figure 7. We note that there is excellent correspondence between the two, as evidenced by the overlap between the similarity solution and the direct numerical computations (the curves in figure 7 are virtually indistinguishable). We observe in figure 6 that an increase in buoyancy flux at the source leads to a broadening of the width of the plume in the unsteady pulse before the new steady state is established. Notably, the velocity field is increased relative to the flow associated with the original buoyancy flux. Together these lead to the surprising variation in the buoyancy flux as it changes from the original value of $\hat{F} = 0.05$ to the new value of $\hat{F} = 1$; the variation is not monotonic, and within the unsteady pulse the buoyancy flux overshoots

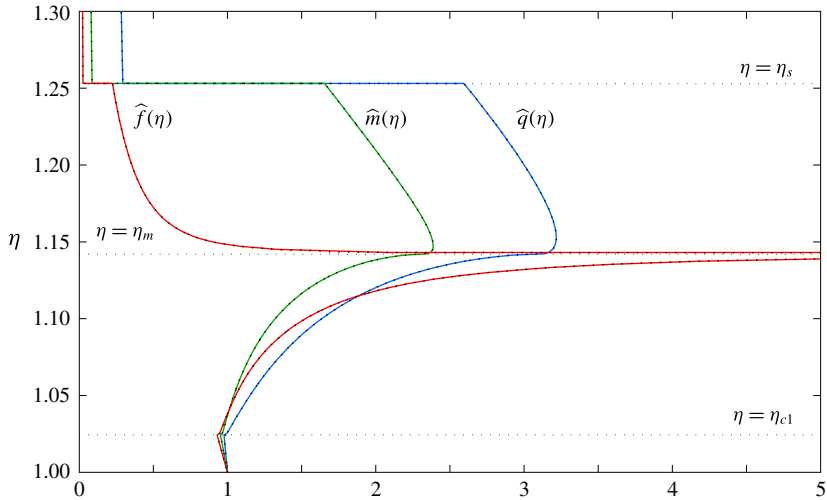


FIGURE 7. (Colour online) The similarity solution for the volume flux, $\hat{q}(\eta)$, the momentum flux, $\hat{m}(\eta)$, and the buoyancy flux, $\hat{f}(\eta)$, as functions of the similarity variable η for shape factor $S = 1.1$ and an increase in the source buoyancy flux $\mathcal{F} = 0.05$ (plotted with solid lines). Also plotted are results from the direct numerical integration of the governing equations (dashed lines), although the two sets of curves are so close in values that they are virtually indistinguishable. The values η_{c1} , η_m and η_s are also marked. These correspond respectively to the boundary between the time-dependent part of the solution and the steady state associated with the new buoyancy flux at the source, the location of a contact discontinuity and the location of a shock that marks the interface between the unsteady evolution and the steady state associated with the original buoyancy flux at the source.

its new value before subsequently decreasing to attain it (see figure 6c). The similarity structure is plotted in figure 7, where the similarity variables are plotted between the leading and trailing edges of the unsteady region. These correspond to a shock at $\eta = \eta_s$ and a point where the gradient changes discontinuously at $\eta = \eta_{c1}$. In between there is a contact discontinuity at $\eta = \eta_m$ where the volume and momentum fluxes are continuous, and the buoyancy flux is unbounded.

6.2. Decrease in buoyancy flux

When the buoyancy flux decreases relatively weakly ($\mathcal{F} < \mathcal{F}_m = 6.9$), we construct the similarity solution between the two critical points, η_{c1} and η_{c2} , given by (6.11) and (6.13) respectively. For $\eta > \eta_{c2}$ the solution corresponds to the steady state associated with the original buoyancy flux, whereas for $\eta < \eta_{c1}$ the solution corresponds to the steady state associated with the new buoyancy flux. As described above, the boundaries between the steady states and this unsteady pulse are characteristics that propagate at the fastest and slowest rates. At some point η_m ($\eta_{c1} < \eta_m < \eta_{c2}$) the similarity solution reaches a state in which $\hat{q}/\hat{m} = 4/3$ and there is a contact discontinuity.

We construct the solutions as follows. We integrate from $\eta = \eta_{c1}$, initiating the numerical solver with the local expansion derived in appendix D, which entails an adjustable constant, $C_{\sigma 1}$. We numerically integrate until $\eta = \eta_{m1}$, at which point $\hat{q}/\hat{m} = 4/3$. We also numerically integrate from $\eta = \eta_{c2}$, initiating the solution using a local

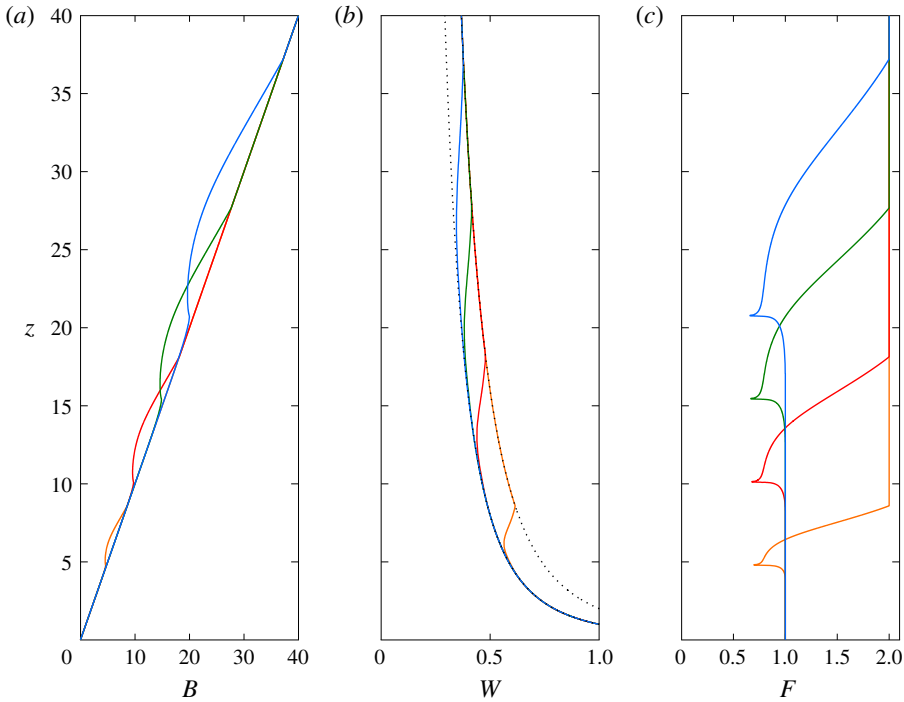


FIGURE 8. (Colour online) The scaled width, $B(z) = z\widehat{Q}/\sqrt{\widehat{M}}$, the scaled velocity, $W(z) = z^{-1/3}\widehat{M}/\widehat{Q}$, and the buoyancy flux, F , as functions of the distance from source, z , at dimensionless times $t = 4.5$ (orange), $t = 9.5$ (red), $t = 14.5$ (green) and $t = 19.5$ (blue) for a decrease in buoyancy flux ($\mathcal{F} = 2$) at $t = 0$ and with shape factor $S = 1.1$. In (b) the scaled velocity $W = z^{-1/3}$, corresponding to the steady velocity field of the original buoyancy flux at the source, and the scaled velocity $W = z^{-1/3}2^{-1/3}$, corresponding to the steady velocity field associated with the new buoyancy flux, are plotted with dashed lines.

expansion derived in appendix D, which features another adjustable constant $C_{\sigma 2}$. We integrate until $\eta = \eta_{m2}$, at which point $\widehat{q}/\widehat{m} = 4/3$. The solution is then found by iteratively adjusting $C_{\sigma 1}$ and $C_{\sigma 2}$ until $\eta_{m1} = \eta_{m2}$ and $\widehat{q}(\eta_{m1}) = \widehat{q}(\eta_{m2})$.

The numerical results from direct integration of the governing partial differential equations are plotted at various instances of time in figure 8. Here, we observe that the volume and momentum fluxes evolve continuously, in contrast to the evolution following an increase in source strength (§ 6.1). During the unsteady evolution from the original state to the new one, the radius of the plume decreases and the velocity increases. The buoyancy flux, however, does not monotonically vary from the new value ($\widehat{F} = 1$) to its original value ($\widehat{F} = 2$). Instead, it initially decreases (see figure 8c). The similarity solution for the unsteady pulse is plotted in figure 9 between the leading and trailing characteristics ($\eta_{c1} < \eta < \eta_{c2}$). This solution features a contact discontinuity at $\eta = \eta_m$, although the mass and momentum fluxes remain continuous at this point. In figure 9 we have plotted both the similarity solution and the rescaled results from the direct numerical integration of the governing equations, and we note that the curves for each of the fields are indistinguishable in this plot.

The morphology of the solution changes for larger decreases in the buoyancy flux. When $\mathcal{F} > \mathcal{F}_m$ we find that the similarity solution features another critical point at

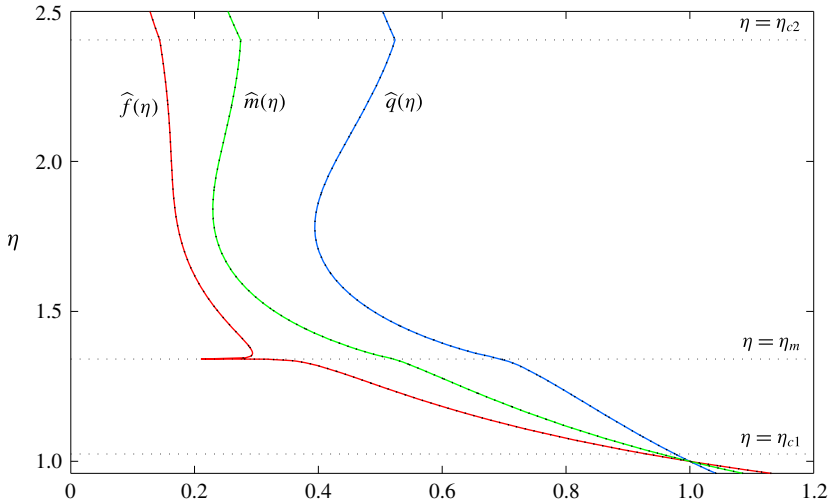


FIGURE 9. (Colour online) The similarity solution for the volume flux, $\hat{q}(\eta)$, the momentum flux, $\hat{m}(\eta)$, and the buoyancy flux, $\hat{f}(\eta)$, as functions of the similarity variable η for shape factor $S = 1.1$ and a decrease in the source buoyancy flux $\mathcal{F} = 2$ (plotted with solid lines). Also plotted are results from the direct numerical integration of the governing equations (dashed lines), although the two sets of curves are so close in values that they are virtually indistinguishable. The values η_{c1} , η_m and η_{c2} are also marked. These correspond respectively to the boundary between the time-dependent part of the solution and the steady state associated with the new buoyancy flux at the source, the location of a contact discontinuity and the location of the interface between the unsteady evolution and the steady state associated with the original buoyancy flux at the source.

$\eta = \eta_{c3}$ at which $\det(\mathbf{D})$ vanishes and the system potentially becomes singular. Local analysis of the behaviour close to this new critical point indicates that non-integer powers in the series expansion are not possible here; the determined power σ is negative, and so in order to ensure that the fields are bounded, we must enforce $C_{\sigma 3} = 0$. This implies that the dependent variables pass smoothly through this critical point. However, having attained a state in which $\hat{q}/\hat{m} > 4(S + \sqrt{S(S-1)})/3$, the only way to connect to the rest of the solution is via an internal shock at $\eta = \eta_s$. Our method for constructing the solution then proceeds as follows. We integrate numerically from the critical point at $\eta = \eta_{c1}$, initiating the solution using the local series expansion about this point and introducing an adjustment constant, $C_{\sigma 1}$, to a location $\eta = \eta_{m1}$ at which there is a contact discontinuity ($\hat{q}/\hat{m} = 4/3$). We also numerically integrate from $\eta = \eta_{c2}$, initiating the solution using the series expansion with constant $C_{\sigma 2}$. This constant is adjusted so that an internal critical point is reached at $\eta = \eta_{c3}$ ($\eta_{c3} < \eta_{c2}$), where we enforce the solvability condition given in (D4). We may then integrate further; we smoothly pass through the critical point and insert a shock at $\eta = \eta_s < \eta_{c3}$, and then integrate until $\hat{q}/\hat{m} = 4/3$ at $\eta = \eta_{m2}$. This leaves two adjustable constants, namely $C_{\sigma 1}$ and η_s , which are iteratively adjusted until $\eta_{m1} = \eta_{m2}$ and $\hat{q}(\eta_{m1}) = \hat{q}(\eta_{m2})$ to give the complete solution.

The results from the numerical integration of the governing equations are plotted in figure 10 for a large decrease in buoyancy flux at various instances of time. We note that, as with the weaker decreases in flux, the plume responds by narrowing

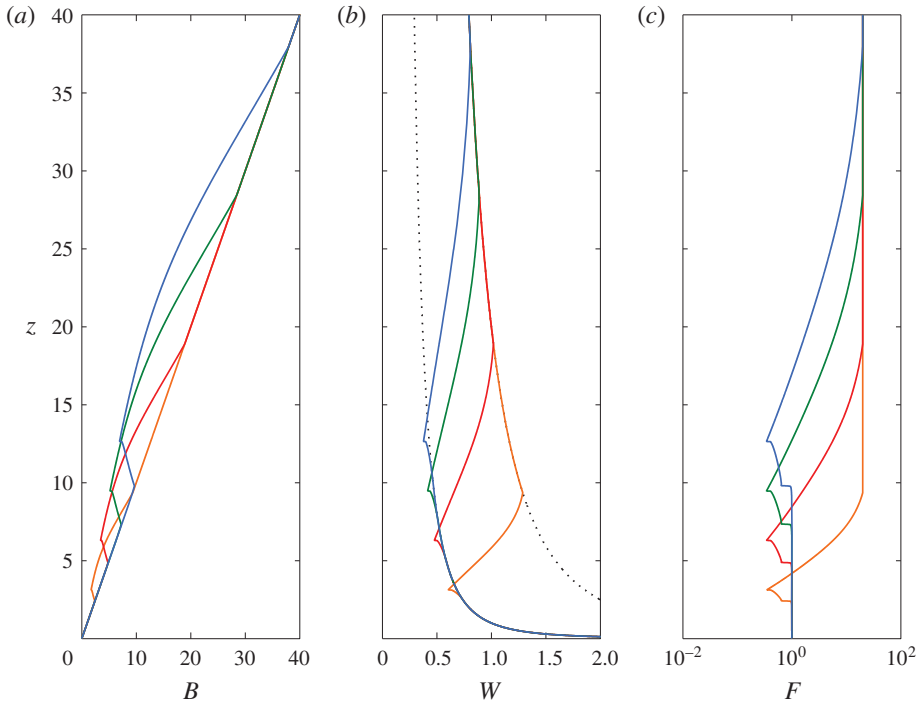


FIGURE 10. (Colour online) The scaled width, $B(z) = z\widehat{Q}/\sqrt{\widehat{M}}$, the scaled velocity, $W(z) = z^{-1/3}\widehat{M}/\widehat{Q}$, and the buoyancy flux, F , as functions of the distance from source, z , at dimensionless times $t = 4.5$ (orange), $t = 9.5$ (red), $t = 14.5$ (green) and $t = 19.5$ (blue) for a decrease in buoyancy flux $\mathcal{F} = 20$ at $t = 0$ and with shape factor $S = 1.1$. In (b) the scaled velocity $W = z^{-1/3}$, corresponding to the steady velocity field of the original buoyancy flux at the source, and the scaled velocity $W = z^{-1/3}20^{-1/3}$, corresponding to the steady velocity field associated with the new buoyancy flux, are plotted with dashed lines.

and accelerating in order to adjust back to its original state. However, an internal shock is also developed. For these parameter values ($\mathcal{F} = 20$ and $S = 1.1$) the shock is of relatively small magnitude, and it generates discontinuities in the velocity and width fields, with the reduced gravity remaining continuous. From this figure it is not possible to observe the presence of the internal critical point ($\eta = \eta_{c3}$) because all of the variables and their derivatives are continuous. However, it can be confirmed that there is an internal region within which $\widehat{q}/\widehat{m} > 4(S + \sqrt{S(S-1)})/3$. The associated similarity solution within the unsteady pulse is plotted in figure 11. As with the weaker decrease in buoyancy flux, this plot features continuous transitions at the leading and trailing edges ($\eta = \eta_{c1}$ and $\eta = \eta_{c2}$ respectively) and a contact discontinuity ($\eta = \eta_m$). Additionally, there is an internal critical point ($\eta = \eta_{c3}$) and an internal shock ($\eta = \eta_s$). The rescaled results from the numerical integration of the governing equations are overlain on the similarity solutions, and again they are virtually indistinguishable, confirming the presence of this similarity solution in the unsteady dynamics of the plume model.

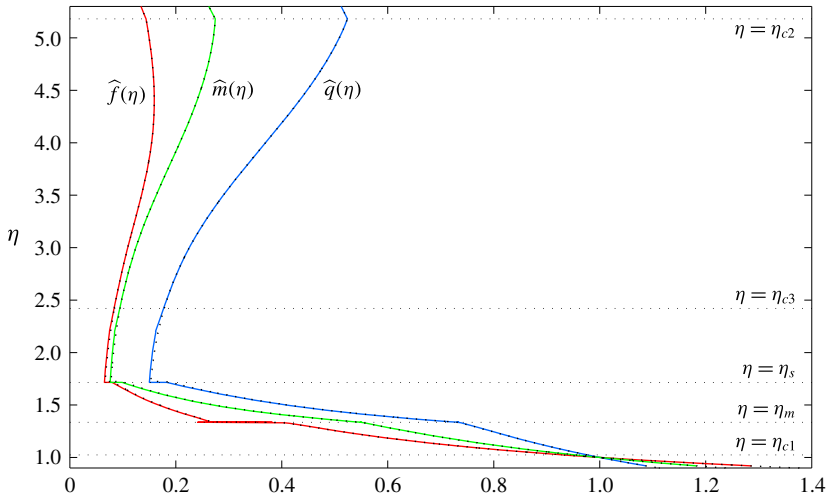


FIGURE 11. (Colour online) The similarity solution for the volume flux, $\hat{q}(\eta)$, the momentum flux, $\hat{m}(\eta)$, and the buoyancy flux, $\hat{f}(\eta)$, as functions of the similarity variable η for shape factor $S=1.1$ and a decrease in the source buoyancy flux $\mathcal{F}=20$ (plotted with solid lines). Also plotted are results from the direct numerical integration of the governing equations (dashed lines), although the two sets of curves are so close in values that they are virtually indistinguishable. The values η_{c1} , η_m , η_s , η_{c3} and η_{c2} are also marked. These correspond respectively to the boundary between the time-dependent part of the solution and the steady state associated with the new buoyancy flux at the source, the location of a contact discontinuity, the location of an internal shock between flow states, the location of a continuous transition and the location of the interface between the unsteady evolution and the steady state associated with the original buoyancy flux at the source.

7. Discussion and conclusion

Steady plume models are applicable on time scales that are long compared with the eddy turnover time that characterizes transient turbulent features, and on time scales shorter than the characteristic time for source variations (Scase *et al.* 2006*b*). In many applications, the effect of variations of the source fluxes of mass, momentum or buoyancy on the plume dynamics is of fundamental importance. Here, unsteady models are essential. For an example, during volcanic eruptions the source conditions can fluctuate in time due to unsteadiness in the physical processes occurring in the volcanic conduit and at the vent. End members of the source unsteadiness are the initiation phase (when an eruption first produces material that becomes buoyant and ascends through the atmosphere) and the waning phase (when the eruption comes to an end through either a gradual reduction in the rate at which material is erupted or an abrupt cessation of the activity) of the eruption.

The unsteady model of turbulent plumes analysed by Scase *et al.* (2006*b*) and Scase (2009) identified a key feature of the unsteady response of plumes to abrupt changes in the source buoyancy flux: the plume adjusts to the new source conditions through a ‘pulse’ that propagates through the plume. However, the model of Scase *et al.* (2006*b*) adopts top-hat profiles for the mean axial velocity and was shown to be ill-posed in the analysis of Scase & Hewitt (2012), with the numerical solutions of Scase *et al.* (2006*b*) and Scase (2009) attained only due to significant numerical viscosity.

The diffusive regularization of the unsteady model proposed by Scase & Hewitt (2012) has an intuitive physical basis: turbulent eddies have a vertical length scale over which different levels of the plume are connected. Numerical solutions (Scase & Hewitt 2012) suggest that the phenomenological model of the turbulent diffusion of momentum advocated by Scase & Hewitt (2012) results in a well-posed unsteady model, but the analysis presented here shows that this modification of the governing system of equations renders the classical power-law solution for steady plumes unstable. As the power-law solutions have strong empirical support (e.g. Morton *et al.* 1956; Papanicolaou & List 1988; Shabbir & George 1994), we conclude that the diffusive regularization of Scase & Hewitt (2012) is not appropriate.

Our analysis identifies a different physical process, a difference in the rates of transport of the cross-sectionally averaged mass and momentum of the plume (referred to as type I dispersion by Craske & van Reeuwijk 2015a,b) which occurs due to non-uniform radial profiles of the mean axial velocity in the plume, and we have shown that including this process through a momentum shape factor leads to a well-posed system of equations. However, this requires the top-hat description of the radial profiles for the axial velocity in the plume, which has been applied extensively (for convenience) in models of steady plumes, to be replaced with a description of the radial variation. The resulting integral model for unsteady plumes introduces only one additional parameter, the momentum shape factor, over the classical steady plume model (Morton *et al.* 1956). Furthermore, the (ensemble averaged) radius of the plume remains dependent on the entrainment coefficient alone, so the unsteady model does not preclude calibration of the entrainment coefficient from laboratory experiments that measure the steady plume width (or spreading angle). To determine the momentum shape factor, the radial profile of the axial velocity can be measured directly (e.g. Papanicolaou & List 1988; Shabbir & George 1994), and the shape factor computed from (2.6).

Explicitly including a momentum shape factor that differs from unity results in a strictly hyperbolic system of equations that governs the plume dynamics. This is appealing, as laboratory experiments (Scase *et al.* 2008) and numerical modelling (Scase *et al.* 2009) show that the adjustment of the plume to changes in the source conditions occurs through the propagation of an unsteady pulse, as predicted by our non-diffusive hyperbolic model. The development of the unsteady pulse following an abrupt change in the source buoyancy flux is described by a similarity solution of the hyperbolic system of equations. The construction of the similarity solution allows us to identify three qualitatively different regimes of the unsteady evolution. Following an increase in the source buoyancy flux, the pulse takes the form of a localized increase in the plume width with a leading discontinuity. If the source buoyancy flux is reduced then the plume width narrows. For a relatively strong reduction in the source buoyancy flux an internal shock occurs in the similarity solution, whereas no internal shock is found if the source buoyancy flux is reduced by a smaller amount. We expect that diffusive processes that are not represented in our formulation will act to locally smooth the sharp gradients that appear in solutions of the hyperbolic model. However, hyperbolic models have been shown to capture the dominant flow dynamics in many settings (Whitham 1974).

Craske & van Reeuwijk (2015a) identify, from direct numerical simulations, the dispersion of momentum as a fundamental feature of turbulent jets, and construct an integral model to describe unsteady jets which includes a description of the non-uniform radial profile of the vertical velocity (Craske & van Reeuwijk 2015b) through shape factors. In the model of Craske & van Reeuwijk (2015b) the integral

conservation equations are derived from the point-wise momentum and energy conservation equations, following the approach of Priestley & Ball (1955), and an energy shape factor rather than a momentum shape factor is introduced. The resulting system of integral conservation equations shares some features with the unsteady integral model proposed here (albeit for a jet rather than a plume), in particular the hyperbolic structure of the system of equations.

For jets the momentum of the flow as it is ejected from a source drives the motion, and there is significant evolution of the radial profile of the axial velocity (referred to as type II dispersion by Craske & van Reeuwijk 2015a,b) as the flow develops away from the source. The evolution of the shape of the radial profiles of axial velocity and buoyancy has been incorporated into a non-constant entrainment coefficient by Kaminski *et al.* (2005) and Carazzo *et al.* (2006). Furthermore, in the unsteady integral model of Craske & van Reeuwijk (2015b) the deviation of the radial profiles from self-similar forms gives rise to diffusive terms in the system of integral conservation equations. Our analysis shows that a description of momentum dispersion, through a shape factor that differs from unity, is sufficient to obtain a well-posed model of unsteady plumes. Therefore, while for jets it is necessary to account for the evolution of the radial profile of axial velocity to self-similar form, for unsteady pure plumes the classical entrainment closure of Morton *et al.* (1956) remains applicable.

The mathematical model we present allows predictions of unsteady plume dynamics to be made and, while our study has focused on changes to the source buoyancy flux, the effect of general temporal variations in the source conditions can be examined. Furthermore, our framework can be applied to describe the unsteady dynamics of plumes in industrial and environmental settings, where additional physical processes such as an ambient flow, thermodynamics and particle transport have a strong influence on the evolution of the plume.

Acknowledgements

We are grateful to Professor R. R. Kerswell, Dr C. G. Johnson and Dr R. E. Hewitt for valuable discussions, and to Dr M. M. Scase and two anonymous referees for suggestions that have improved this contribution. This project has received funding from the European Union's Seventh Programme for research, technological development and demonstration under grant agreement no. 308377 and from the NERC through grant NE/I01554X/1.

Appendix A. Evolution of energy for unsteady plumes

In the derivation of our integral model for unsteady plumes we made direct use of the point-wise continuity equation to obtain an integral equation for conservation of mass, following the approach used by Morton *et al.* (1956) for steady plumes. This requires *a priori* a choice to be made for a representative plume radius, b , and an entrainment closure to describe the mixing of ambient fluid into the plume.

An alternative approach, pioneered by Priestley & Ball (1955) for steady flows and developed by Fox (1970), Kaminski *et al.* (2005) and Carazzo *et al.* (2006), is to substitute the expression of the evolution of axial kinetic energy for the continuity equation in the set of point-wise conservation equations. As the equation for conservation of axial kinetic energy is derived as an (axial velocity) moment of the equation for the conservation of axial momentum, rewritten in conservation form through application of the continuity equation, taking the conservation of axial kinetic

energy together with the conservation of axial momentum provides no additional information over the set of point-wise conservation equations with continuity and conservation of axial momentum (see Morton 1971, for a detailed discussion). The integral expression for conservation of axial momentum and conservation of axial kinetic energy can be manipulated into a form that expresses conservation of mass in the integral sense, and, from this, an expression for turbulent entrainment is obtained (Priestley & Ball 1955; Fox 1970; Morton 1971; Kaminski *et al.* 2005; Carazzo *et al.* 2006). However, the integral equations that result from the use of the conservation of axial kinetic energy differ from those obtained when the continuity equation is used directly. Indeed, the differences occur due to the application of turbulent closures in different terms following the cross-sectional integration of the point-wise conservation equations: in the approach of Morton *et al.* (1956) the turbulence closure is applied as an inflow velocity in the kinematic condition applied at the plume boundary, whereas the closure is applied to the turbulent fluctuation terms that occur in the conservation of axial momentum equation when the approach of Priestley & Ball (1955) is used. Finally, as noted by Morton (1971), both closures introduce parameters that can only be determined empirically.

Recently, Craske & van Reeuwijk (2015a,b) used the conservation of axial kinetic energy in place of the continuity equations in the set of point-wise conservation equations in their model of unsteady jets. In this appendix we adopt a similar approach for buoyant plumes. We note that our approach differs as we again specify the plume radius $r = b(z, t)$ as a measurable surface in the plume and introduce shape factors to account for non-uniform radial profiles of mean flow quantities. Thus, we define the volume flux, axial momentum flux and the flux of mean axial kinetic energy as

$$b^2W = 2 \int_0^b r\bar{w} dr, \quad S_m b^2W^2 = 2 \int_0^b r\bar{w}^2 dr \quad \text{and} \quad S_e b^2W^3 = 2 \int_0^b r\bar{w}^3 dr \quad (\text{A } 1a-c)$$

respectively, where, in (A 1c), S_e is an energy flux shape factor.

Integration of the point-wise Reynolds-averaged conservation equations for axial momentum (2.1b), axial kinetic energy (see Craske & van Reeuwijk 2015a) and reduced gravity (2.1c) gives the following set of integral equations:

$$\frac{\partial}{\partial t}(b^2W) + \frac{\partial}{\partial z}(S_m b^2W^2) = b^2G' - \frac{\partial}{\partial z}(M_f + M_p), \quad (\text{A } 2a)$$

$$\frac{\partial}{\partial t}(S_m b^2W^2) + \frac{\partial}{\partial z}(S_e b^2W^3) = 2S_f b^2G'W + (P_m + P_f + P_p) - \frac{\partial}{\partial z}(E_f + E_p), \quad (\text{A } 2b)$$

$$\frac{\partial}{\partial t}(b^2G') + \frac{\partial}{\partial z}(S_f b^2G'W) = -\frac{\partial B_f}{\partial z}, \quad (\text{A } 2c)$$

where, following Craske & van Reeuwijk (2015a,b), the correlation fluctuation terms and non-hydrostatic pressure terms, which are formally higher order in the plume slenderness, R/H , than the mean fluxes, are retained and given by

$$\left. \begin{aligned} M_f &= 2 \int_0^b r\overline{w'^2} dr, & M_p &= 2 \int_0^b r\bar{p} dr, & E_f &= 4 \int_0^b r\overline{w'^2} \frac{\partial \bar{w}}{\partial z} dr, \\ E_p &= 4 \int_0^b r\bar{p}\bar{w} dr, & P_m &= 4 \int_0^b r\overline{u'w'} \frac{\partial \bar{w}}{\partial r} dr, & P_f &= 4 \int_0^b r\overline{w'^2} \frac{\partial \bar{w}}{\partial z} dr, \\ P_p &= 4 \int_0^b r\bar{p} \frac{\partial \bar{w}}{\partial z} dr, & B_f &= 2 \int_0^b r\overline{g'_r w'} dr. \end{aligned} \right\} \quad (\text{A } 3)$$

Here, \bar{p} denotes the averaged deviation of the pressure in the plume from hydrostatic pressure. It should be noted that in (A 2) we have neglected terms in which flow quantities are evaluated on the plume boundary.

Manipulation of the integral equations for conservation of axial momentum (A 2a) and conservation of axial kinetic energy (A 2b) leads to an expression akin to conservation of mass,

$$\frac{S_m}{S_e} \frac{\partial}{\partial t}(b^2) + \frac{\partial}{\partial z}(b^2W) = 2\alpha_e bW, \tag{A 4}$$

where the entrainment rate α_e is given by

$$\begin{aligned} \alpha_e = & \left(\frac{S_m - S_f}{S_e} \right) \frac{bG'}{W^2} + \frac{1}{bW^2} \left(\frac{1}{S_m} - \frac{S_m}{S_e} \right) \frac{\partial}{\partial z}(S_m b^2 W^2) + \frac{b}{2S_e W} \frac{\partial S_m}{\partial t} + \frac{S_m^2}{2S_e} \frac{\partial}{\partial z} \left(\frac{S_e}{S_m^2} \right) \\ & - \frac{P_m + P_p + P_f}{2S_e bW^3} - \frac{S_m}{S_e bW^2} \frac{\partial}{\partial z}(M_f + M_p) + \frac{1}{2S_e bW^3} \frac{\partial}{\partial z}(E_f + E_p). \end{aligned} \tag{A 5}$$

The form of the mass conservation (A 4) is similar to the expression proposed by Craske & van Reeuwijk (2015a,b), but differs due to different choices for the plume width. The entrainment rate has a similar form to that of Craske & van Reeuwijk (2015a,b) for jets, although in (A 5) the first term on the right-hand side does not appear for jets where $G' \equiv 0$. A similar term, which results in an entrainment rate that depends on the local Richardson number of the plume (given by $Ri = bG'/W^2$), occurs in the entrainment rate in the models that adopt the approach of Priestley & Ball (1955) (e.g. Priestley & Ball 1955; Fox 1970; Kaminski *et al.* 2005; Carazzo *et al.* 2006), and has been shown to be important when describing the near-source development of buoyant jets into plumes (Kaminski *et al.* 2005; Carazzo *et al.* 2006; Ezzamel *et al.* 2015). Further, the entrainment rate here includes a contribution from temporal changes in the momentum shape factor that does not appear in the entrainment rate of Craske & van Reeuwijk (2015a,b).

For turbulent plumes from pure-plume sources at distances sufficiently far from the source, experiments suggest that the radial profiles of the mean axial velocity and reduced gravity, and the second-order turbulent velocity statistics, have reached a self-similar form (Ezzamel *et al.* 2015). The shape factors can then be taken as constant values. Furthermore, following Craske & van Reeuwijk (2015b) and for simplicity, we take the turbulent production and transport terms and non-hydrostatic pressure terms to be such that the entrainment rate is given by

$$\alpha_e \approx \alpha_0 + \left(\frac{S_m - S_f}{S_e} \right) \frac{bG'}{W^2} + \frac{1}{bW^2} \left(\frac{1}{S_m} - \frac{S_m}{S_e} \right) \frac{\partial}{\partial z}(S_m b^2 W^2), \tag{A 6}$$

with α_0 constant.

Steady solutions of the plume model with the non-constant entrainment rate (A 6) with pure-plume boundary conditions ($Q(0) = 0, M(0) = 0, F(0) = F_0$) are given by

$$Q = \frac{6\alpha_0}{5} \left(\frac{9\alpha_0}{10} \right)^{1/3} \left(\frac{F_0}{S_m} \right)^{1/3} \left[1 - \frac{8S_m}{5S_e}(S_m - S_m^2 - S_f + S_e) \right]^{-4/3} z^{5/3}, \tag{A 7a}$$

$$M = \left(\frac{9\alpha_0}{10} \right)^{2/3} \left(\frac{F_0}{S_m} \right)^{2/3} \left[1 - \frac{8S_m}{5S_e}(S_m - S_m^2 - S_f + S_e) \right]^{-2/3} z^{4/3}, \tag{A 7b}$$

$$F = F_0. \tag{A 7c}$$

Therefore, the non-constant entrainment coefficient does not change the spatial variation of the steady solutions, although the prefactors in the power-law forms are changed from the Morton *et al.* (1956) solutions, unless the shape factors take values such that $S_m^2 - S_m - S_e + S_f = 0$, which occurs for $S_m = 1$ and $S_e = S_f$. We note that the factors could diverge if $1 - 8S_m(S_m - S_m^2 - S_f + S_e)/5S_e = 0$. The radius of the plume for the non-constant entrainment coefficient is given by

$$b = \frac{6\alpha_0}{5} \left[1 - \frac{8S_m}{5S_e} (S_m - S_m^2 - S_f + S_e) \right]^{-1} z, \quad (\text{A } 8)$$

and so the plume radius increases linearly with height as in the model of Morton *et al.* (1956). However, in contrast to the model with a constant entrainment coefficient, the spreading angle of the plume depends on the shape factors for momentum, buoyancy and energy (unless $S_m^2 - S_m - S_e + S_f = 0$).

An alternative approach is to augment the system of integral equations (A 2) with the integral expression for conservation of mass (2.10a). We can then interpret the integral expression for conservation of axial kinetic energy as governing the evolution of the momentum shape factor, and, in order to fully specify this evolution, a closure is required to describe the evolution of the energy shape factor. A higher velocity moment of the point-wise conservation equations for mass and momentum would provide an integral equation governing the evolution of the energy shape factor, but would, of course, introduce a new shape factor. Therefore, a turbulence closure must be invoked at some level within the hierarchy of equations. Laboratory experiments (e.g. Papanicolaou & List 1988; Wang & Law 2002; Ezzamel *et al.* 2015) suggest that the momentum shape factor can be taken as a constant value for fully developed turbulent plumes sufficiently far from the source, and this represents a turbulence closure at the level of conservation of mass, momentum and buoyancy.

Appendix B. A phase-plane analysis of steady solutions of the plume model with diffusive terms

In § 3 the steady solutions of the integral model for unsteady plumes with phenomenological diffusive terms included to describe turbulent mixing by eddy diffusion were shown to be linearly unstable to small perturbations. Therefore, while steady solutions of the diffusive system of equations can be found analytically (see (3.3)) and are modifications of the well-known steady solutions given by Morton *et al.* (1956), the solutions cannot be realized. However, the linear stability analysis in § 3 does not investigate other possible steady states. In particular, it could be possible that other steady solutions that do not enforce pure-plume boundary conditions exist, and that these could be attracting states for the steady diffusive system of equations.

Here, we examine the steady plume equations with diffusive terms by treating the system of equations as a dynamical system. To this end, we allow the volume flux Q to be the independent variable in the system rather than the distance from the source. We note that in an unstratified ambient the buoyancy flux is conserved, and so $F \equiv F_0$, with F_0 a specified constant.

We consider first the diffusive term proposed by Scase & Hewitt (2012) (as given in the unsteady momentum conservation equation (3.2)). The equation for the conservation of mass in the steady state allows us to write

$$\frac{d}{dz} = 2\alpha M^{1/2} \frac{d}{dQ}, \quad (\text{B } 1)$$

and therefore, from the conservation of momentum, we find

$$\kappa Q^2 \frac{d^2M}{dQ^2} + \kappa \frac{Q^2}{M} \frac{dM^2}{dQ} + (3\kappa + S)Q \frac{dM}{dQ} + 2\kappa M = -\frac{F_0}{2\alpha} \frac{Q^2}{M^{3/2}}, \tag{B 2}$$

here treating M as a function of Q . Equation (B 2) can be further manipulated by introducing new dependent variables

$$X = Q^{-4/5}M(Q) \quad \text{and} \quad Y = Q^{1/5} \frac{dM}{dQ} - \frac{4}{5}Q^{-4/5}M(Q), \tag{B 3a,b}$$

and an independent variable ξ , with $Q = \exp(\xi)$, which allows the system to be written as the following autonomous system:

$$\frac{dX}{d\xi} = Y, \tag{B 4a}$$

$$\kappa \frac{dY}{d\xi} + \kappa \frac{Y^2}{X} - \left(\frac{4\kappa}{5} + S\right)Y + \left(\frac{2\kappa}{25} - \frac{4S}{5}\right)X = -\frac{F_0}{2\alpha}X^{-3/2}. \tag{B 4b}$$

The coupled nonlinear system (B 4) has a single fixed point at $Y = 0$ and $X = X_0$ with

$$X_0 = \left(\frac{5F_0}{8\alpha(S - \kappa/10)}\right)^{2/5}, \tag{B 5}$$

which, after returning to the original variables, is the steady solution given by (3.3). However, other solutions of the autonomous system for arbitrary initial conditions can be readily found by numerically integrating the system (B 4). The trajectories in the phase plane corresponding to solutions of (B 4) with a momentum shape factor $S = 1$ are shown in figure 12. We see that the fixed point is a saddle with two stable trajectories (such that initial conditions precisely on these trajectories converge to the fixed point) and two unstable trajectories. For initial conditions that are perturbed away from the pure-plume conditions (i.e. $Q(z = 0) = M(z = 0) = 0$) at the fixed point, the trajectories move the solution away from the fixed point and we find either $M(Q) \rightarrow 0$ or $M(Q) \rightarrow \infty$ along the phase-plane trajectories. Taking a momentum shape factor that differs from unity does not change the topology of the trajectories in the phase plane (figure 13).

A local analysis of trajectories that are perturbed away from the fixed point reproduces the results of the linear stability analysis (3.6). Indeed, taking $X = X_0 + X_1(\xi)$ and $Y = Y_1(\xi)$ with $|X_1| \ll 1$ and $|Y_1| \ll 1$, we find

$$\frac{d}{d\xi} \begin{pmatrix} X_1 \\ Y_1 \end{pmatrix} = \begin{pmatrix} 0 & 1 \\ 1/5 + 2S/\kappa & 4/5 + S/\kappa \end{pmatrix} \begin{pmatrix} X_1 \\ Y_1 \end{pmatrix}, \tag{B 6}$$

and the eigenvalues of the Jacobian matrix are

$$a_{\pm} = \frac{5S + 4\kappa \pm \sqrt{25S^2 + 240S\kappa - 4\kappa^2}}{10\kappa}. \tag{B 7}$$

The corresponding eigenvectors are

$$\mathbf{v}_{\pm} = (1, a_{\pm})^T. \tag{B 8}$$

Therefore, we find $X_1 \sim \exp(a_{\pm}\xi)$.

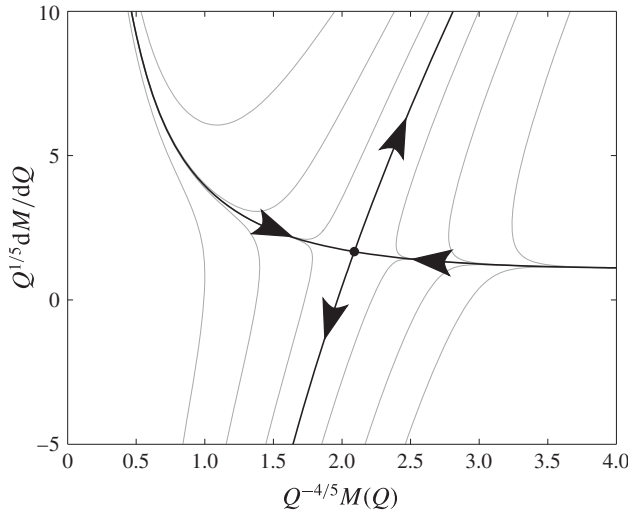


FIGURE 12. Trajectories in the phase plane of solutions to the steady plume equations with the diffusive regularization of Scase & Hewitt (2012) with $F_0 = 1$, $\alpha = 0.1$, $\kappa = 0.1$ and $S = 1$. The autonomous system has a single fixed point (denoted by the black point in the figure) that corresponds to the steady pure-plume solution of Morton *et al.* (1956) with a modification for the diffusive term (given by (3.3)). The fixed point is a saddle, with two stable directions and two unstable directions, shown as bold solid lines in the figure, with arrows denoting the stability of the trajectories. Additional trajectories, corresponding to solutions with non-pure-plume initial conditions, are shown as thin grey lines.

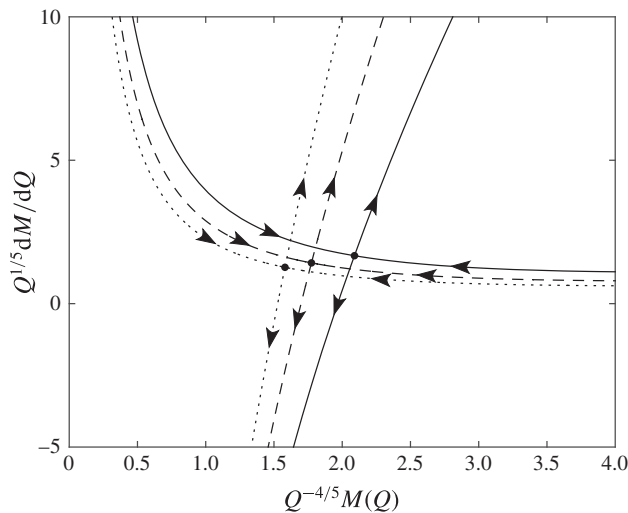


FIGURE 13. The stable and unstable trajectories through fixed points in the phase plane of solutions to the steady plume equations with the diffusive regularization of Scase & Hewitt (2012) with $F_0 = 1$, $\alpha = 0.1$ and $\kappa = 0.1$ for momentum shape factor $S = 1$ (solid lines), $S = 1.5$ (dashed line) and $S = 2.0$ (dotted line).

The analysis presented above can be applied to the alternative form of the eddy diffusion term in the momentum balance given in (3.8) for unsteady conditions.

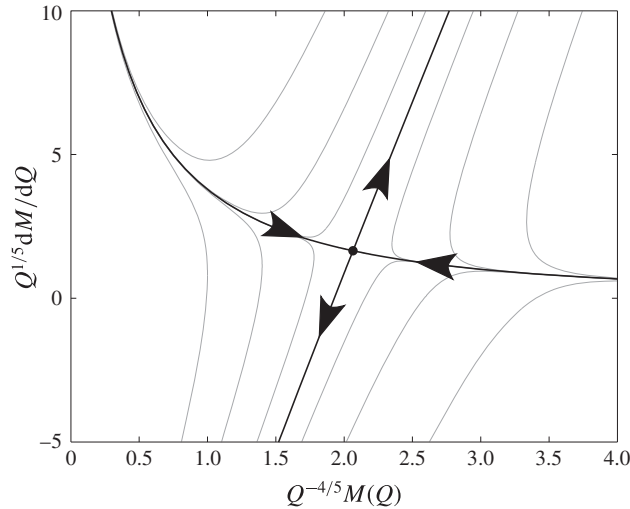


FIGURE 14. Trajectories in the phase plane of solutions to the steady plume equations with the diffusive regularization (3.8) with $F_0 = 1$, $\alpha = 0.1$, $\kappa = 0.1$ and $S = 1$. The autonomous system has a single fixed point (denoted by the black point in the figure) that corresponds to the steady pure-plume solution of Morton *et al.* (1956) with a modification for the diffusive term (given by (3.9)). The fixed point is a saddle, with two stable directions and two unstable directions, shown as bold solid lines in the figure, with arrows denoting the stability of the trajectories. Additional trajectories, corresponding to solutions with non-pure-plume initial conditions, are shown as thin grey lines.

We again find a single fixed point that corresponds to the steady solution (3.9). The topology of trajectories in the phase plane is qualitatively similar to that of the Scase & Hewitt (2012) diffusive term (figures 14 and 15), with the single fixed point being a saddle, and trajectories from arbitrary initial conditions having either $M(Q) \rightarrow 0$ or $M(Q) \rightarrow \infty$ as $Q \rightarrow \infty$. Taking a momentum shape factor that differs from unity does not change the topology of the phase portrait (figure 15).

The conclusion of this analysis is that, for each of the proposed axial diffusion terms ((3.1) and (3.7)), the steady solutions for pure-plume boundary conditions are not stable, and, furthermore, for more general boundary conditions, the steady solutions do not evolve towards the pure-plume solution in the far field. This is in contrast to steady solutions of the non-diffusive system with general boundary conditions, which converge to the pure-plume solution in the far field (Morton 1959; Hunt & Kaye 2001, 2005).

Appendix C. Separable similarity solution

Scase *et al.* (2006b) identified a ‘separable’ similarity solution that emerged as an exact solution to their time-dependent governing equations, and, although it did not satisfy the boundary conditions exactly, it appeared to play a role in ‘organizing’ the underlying dynamics when the buoyancy flux at the origin was abruptly reduced by a relatively large factor. In this appendix we derive the analogue of their solution in our regularized system of governing equations and discuss its relevance for the solutions that arise when the source buoyancy flux is abruptly changed.

The separable solution emerges as a special case of the similarity solutions derived in § 6 and corresponds to a fixed point in the differential system for $(\hat{q}(\eta), \hat{m}(\eta), \hat{f}(\eta))$

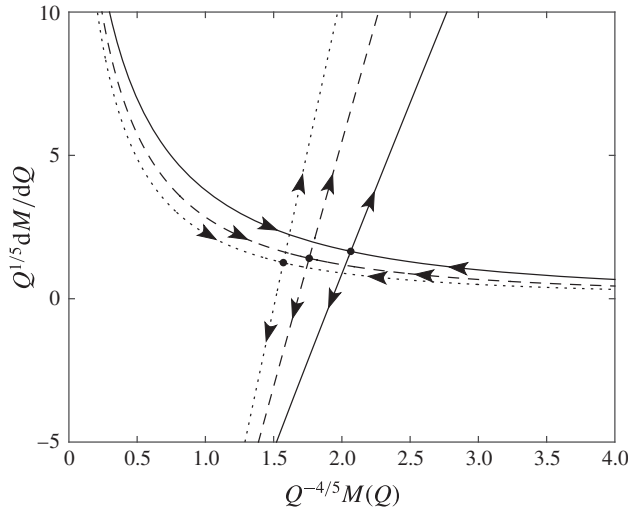


FIGURE 15. The stable and unstable trajectories through fixed points in the phase plane of solutions to the steady plume equations with the diffusive regularization (3.8) with $F_0 = 1$, $\alpha = 0.1$ and $\kappa = 0.1$ for momentum shape factor $S = 1$ (solid lines), $S = 1.5$ (dashed line) and $S = 2.0$ (dotted line).

given by (6.3). Thus, we find that $\hat{q} = \hat{q}_0 \equiv (\hat{q}_0, \hat{m}_0, \hat{f}_0)$ is given by

$$\hat{q}_0 = \frac{25}{162}, \quad \hat{m}_0 = \frac{25}{324} \quad \text{and} \quad \hat{f}_0 = \frac{25}{432} \frac{(2S - 1)}{S}. \tag{C 1a-c}$$

In terms of the original variables this corresponds to

$$Q = \frac{2\alpha^2 z^3}{9t}, \quad M = \frac{\alpha^2 z^4}{9t^2} \quad \text{and} \quad F = \frac{\alpha^2(2S - 1)z^4}{9t^3}. \tag{C 2a-c}$$

Notably, this solution is independent of the source flux of buoyancy.

We may examine the stability of this fixed point in terms of the similarity variable by introducing $\hat{q} = \hat{q}_0 + \hat{q}_1$ and linearizing about the fixed point \hat{q}_0 . This gives

$$\begin{pmatrix} -\frac{8}{3} & 4 & 0 \\ -1 & \frac{4S}{3} & 0 \\ -\frac{3(2S-1)}{4} & \frac{3(2S-1)}{2} & -\frac{2}{3} \end{pmatrix} \eta \frac{d\hat{q}_1}{d\eta} = \begin{pmatrix} -3 & 3 & 0 \\ \frac{3(2S-1)}{2S} & -\frac{3(2S-1)}{S} & 0 \\ 2S & 2(1-4S) & \frac{8S}{3} \end{pmatrix} \hat{q}_1. \tag{C 3}$$

We look for a solution of the form $\hat{q}_1 = \eta^\lambda \tilde{q}$ and deduce that

$$(\lambda + 4S)(64S^2\lambda^2 - 72S^2\lambda - 72S\lambda^2 + 126S\lambda - 162S - 36\lambda + 81) = 0. \tag{C 4}$$

From this condition, we deduce that there is always a root for which $\text{Re}(\lambda) > 0$ when $S > 1$, while there are other roots for which $\text{Re}(\lambda) < 0$. Thus, the fixed point, \hat{q}_0 , is linearly unstable, and this implies that in terms of the similarity variables, while the

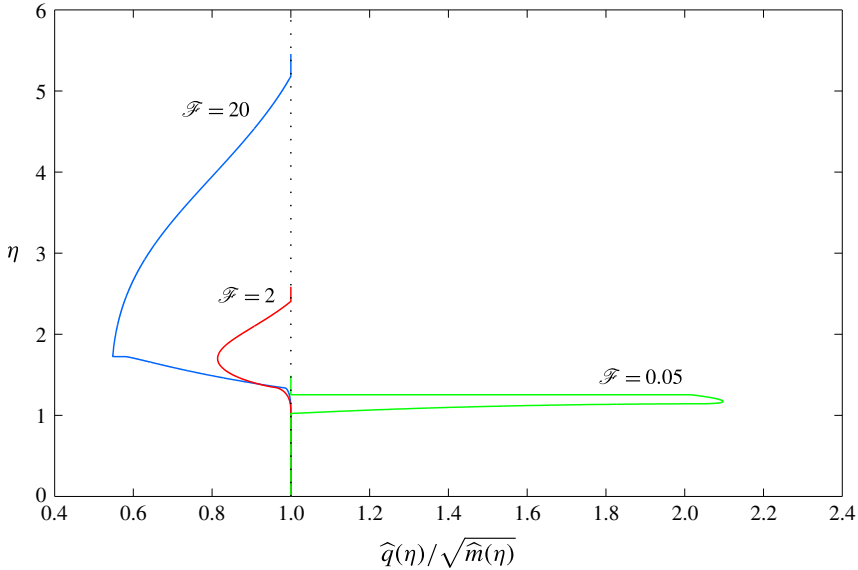


FIGURE 16. (Colour online) The scaled width of the plume, $\hat{q}/\sqrt{\hat{m}}$, as a function of the similarity variable, η , for $\mathcal{F} = 0.05$ (green line), $\mathcal{F} = 2$ (red line) and $\mathcal{F} = 20$ (blue line) and shape factor $S = 1.1$.

solution may approach the fixed point, it does not remain close to it asymptotically as $\eta \rightarrow \infty$. We illustrate this by plotting $\hat{q}/\sqrt{\hat{m}}$ as a function of the similarity variable η for $\mathcal{F} = 20, 2$ and 0.05 (see figure 16). A steady state corresponds to $\hat{q}/\sqrt{\hat{m}} = 1$, while for the separable solution $\hat{q}/\sqrt{\hat{m}} = 5/9$. We note that while the evolution for the strongest decrease in buoyancy flux ($\mathcal{F} = 20$) becomes close to $\hat{q}/\sqrt{\hat{m}} = 5/9$ at one location during its evolution, this separable solution does not in general strongly characterize the entire form of the similarity solution.

Appendix D. Local series expansions at critical points

In this appendix we examine similarity solutions governed by

$$D\eta \frac{d\hat{q}}{d\eta} = \mathbf{b}, \tag{D 1}$$

where \mathbf{D} and \mathbf{b} are the matrix and vector defined in (6.3). We examine the solutions local to a critical point, $\eta = \eta_{ci}$ ($i = 1, 2$), of this differential system, where $\det(\mathbf{D})$ vanishes.

It is convenient to write $\nu = \log(\eta/\eta_{ci})$ and to write the following expansion of the dependent variables, the matrix \mathbf{D} and the forcing vector \mathbf{b} :

$$\hat{\mathbf{q}} = \hat{\mathbf{q}}_0 + \nu \hat{\mathbf{q}}_1 + \nu^2 \hat{\mathbf{q}}_2 + \nu^\sigma \hat{\mathbf{q}}_\sigma + \nu^{\sigma+1} \hat{\mathbf{q}}_{\sigma+1} + \dots, \tag{D 2a}$$

$$\mathbf{D} = \mathbf{D}_0 + \nu \mathbf{D}_1 + \nu^\sigma \mathbf{D}_\sigma + \dots, \tag{D 2b}$$

$$\mathbf{b} = \mathbf{b}_0 + \nu \mathbf{b}_1 + \nu^\sigma \mathbf{b}_\sigma + \dots, \tag{D 2c}$$

where σ is not an integer. This form of expansion series is possible because $\det(\mathbf{D}_0) = 0$. We substitute the series (D 2) into (D 1) and in the regime $\nu \ll 1$

balance terms in powers of ν . At $O(1)$ and at $O(\nu^{\sigma-1})$ we find that

$$\mathbf{D}_0 \hat{\mathbf{q}}_1 = \mathbf{b}_0 \quad \text{and} \quad \sigma \mathbf{D}_0 \hat{\mathbf{q}}_\sigma = 0. \tag{D 3a,b}$$

The matrix \mathbf{D}_0 is singular; thus, we can find vectors \mathbf{e} and $\hat{\mathbf{e}}^T$ such that $\mathbf{D}_0 \mathbf{e} = 0$ and $\hat{\mathbf{e}}^T \mathbf{D}_0 = 0$ respectively. This means that from (D 3a) we deduce the solvability criterion

$$\hat{\mathbf{e}}^T \mathbf{b}_0 = 0, \tag{D 4}$$

and that $\hat{\mathbf{q}}_1 = C_1 \mathbf{e} + \hat{\mathbf{q}}_f$ and $\hat{\mathbf{q}}_\sigma = C_\sigma \mathbf{e}$, where $\hat{\mathbf{q}}_f$ is a particular solution of (D 3a) and C_1 and C_σ are constants. From a balance of terms at $O(\nu)$ and $O(\nu^\sigma)$ we deduce

$$\hat{\mathbf{e}}^T \mathbf{D}_1 \hat{\mathbf{q}}_1 = \hat{\mathbf{e}}^T \mathbf{b}_1 \quad \text{and} \quad \hat{\mathbf{e}}^T (\mathbf{D}_\sigma \hat{\mathbf{q}}_1 + \mathbf{D}_1 \sigma \hat{\mathbf{q}}_\sigma) = \hat{\mathbf{e}}^T \mathbf{b}_\sigma. \tag{D 5a,b}$$

The first of these, (D 5a), determines the value of the constant C_1 , while the second, (D 5b), determines the non-integer power σ .

We may apply this formulation to any of the critical points, but the locations that are of most interest are the boundaries between the steady and unsteady portions of the solution. First, we analyse the local behaviour near to $\eta_{c2} = 4\mathcal{F}^{1/3}(S + \sqrt{S(S-1)})/3$, which corresponds to the boundary between the original source and the unsteady pulse within the similarity solution. At this point the solution is given by

$$\hat{\mathbf{q}}_0 = (\beta_0, \beta_0^2, \beta_0^3), \quad \text{where} \quad \beta_0 = \frac{3}{4}(S + \sqrt{S(S-1)})^{-1}. \tag{D 6}$$

The vectors \mathbf{e} and $\hat{\mathbf{e}}^T$ are given by

$$\mathbf{e}^T = \left(\frac{16}{9}S(2S-1 + 2\sqrt{S(S-1)}), \frac{4}{3}(2S-1 + 2\sqrt{S(S-1)}), 1 \right), \tag{D 7a}$$

$$\hat{\mathbf{e}}^T = \left(-\frac{3}{4}(2S-1 - 2\sqrt{S(S-1)}), 1, 0 \right). \tag{D 7b}$$

The particular solution is given by

$$\hat{\mathbf{q}}_f = (-\beta_0, -2\beta_0^2, -3\beta_0^3), \tag{D 8}$$

the constant $C_1 = 0$ and the exponent, σ , is

$$\sigma = \frac{13}{8} - \frac{5(2S-1)}{16\sqrt{S(S-1)}}. \tag{D 9}$$

The local expansion is bounded as $\nu \rightarrow 0$ provided that $\sigma > 0$, a condition that demands $S > 25/24$. We note that this condition is identical to the criterion for linear stability. Its origin is identical: it comes from the requirement that the unsteady adjustment remains bounded at its leading edge.

The solution at the trailing edge of the unsteady portion of the solution is broadly similar. Expanding the dependent variables close to $\eta_{c1} = 4(S - \sqrt{S(S-1)})/3$, we find that the solution is given by

$$\hat{\mathbf{q}}_0 = (\beta_1, \beta_1^2, \beta_1^3), \quad \text{where} \quad \beta_1 = \frac{3}{4}(S - \sqrt{S(S-1)})^{-1}. \tag{D 10}$$

The particular solution is given by

$$\hat{q}_f = (-\beta_1, -2\beta_1^2, -3\beta_1^3), \quad (\text{D } 11)$$

the constant $C_1 = 0$ and the exponent, σ , is

$$\sigma = \frac{13}{8} + \frac{5(2S-1)}{16\sqrt{S(S-1)}}. \quad (\text{D } 12)$$

REFERENCES

- BAINES, W. D. & TURNER, J. S. 1969 Turbulent buoyant convection from a source in a confined region. *J. Fluid Mech.* **37**, 51–80.
- BENDER, C. M. & ORSZAG, S. 1978 *Advanced Mathematical Methods for Scientists and Engineers*. McGraw-Hill.
- CARAZZO, G., KAMINSKI, E. & TAIT, S. 2006 The route to self-similarity in turbulent jets and plumes. *J. Fluid Mech.* **547**, 137–148.
- CRASKE, J. & VAN REEUWIJK, M. 2013 Robust and accurate open boundary conditions for incompressible turbulent jets and plumes. *Comput. Fluids* **86** (0), 284–297.
- CRASKE, J. & VAN REEUWIJK, M. 2015a Energy dispersion in turbulent jets. Part 1. Direct simulation of steady and unsteady jets. *J. Fluid Mech.* **763**, 500–537.
- CRASKE, J. & VAN REEUWIJK, M. 2015b Energy dispersion in turbulent jets. Part 2. A robust model for unsteady jets. *J. Fluid Mech.* **763**, 538–566.
- DELICHATSIOS, M. A. 1979 Time similarity analysis of unsteady buoyant plumes in neutral surroundings. *J. Fluid Mech.* **93**, 241–250.
- EMANUEL, K. A. 1994 *Atmospheric Convection*. Oxford University Press.
- EZZAMEL, A., SALIZZONI, P. & HUNT, G. R. 2015 Dynamical variability of axisymmetric buoyant plumes. *J. Fluid Mech.* **765**, 576–611.
- FLANDERS, H. 1973 Differentiation under the integral sign. *Am. Math. Mon.* **80** (6), 615–627.
- FOX, D. G. 1970 Forced plume in a stratified fluid. *J. Geophys. Res.* **75** (33), 6818–6835.
- GOTTLIEB, S. & SHU, C.-W. 1998 Total variation diminishing Runge–Kutta schemes. *Math. Comput.* **67** (221), 73–85.
- HOGG, A. J. & PRITCHARD, D. 2004 The effects of hydraulic resistance on dam-break and other shallow inertial flows. *J. Fluid Mech.* **501**, 179–212.
- HUNT, G. R. & VAN DEN BREMER, T. S. 2011 Classical plume theory: 1937–2010 and beyond. *IMA J. Appl. Math.* **76** (3), 424–448.
- HUNT, G. R. & KAYE, N. B. 2005 Lazy plumes. *J. Fluid Mech.* **533**, 329–338.
- HUNT, G. R. & KAYE, N. G. 2001 Virtual origin correction for lazy turbulent plumes. *J. Fluid Mech.* **435**, 377–396.
- JIANG, X. & LUO, K. H. 2000 Direct numerical simulation of the puffing phenomenon of an axisymmetric thermal plume. *Theor. Comput. Fluid Dyn.* **14** (1), 55–74.
- JOSEPH, D. D. & SAUT, J. C. 1990 Short-wave instabilities and ill-posed initial-value problems. *Theor. Comput. Fluid Dyn.* **1** (4), 191–227.
- KAMINSKI, E., TAIT, S. & CARAZZO, G. 2005 Turbulent entrainment in jets with arbitrary buoyancy. *J. Fluid Mech.* **526**, 361–376.
- KAYE, N. B. 2008 Turbulent plumes in stratified environments: a review of recent work. *Atmos. Ocean* **46** (4), 433–441.
- KOH, R. C. Y. & BROOKS, N. H. 1975 Fluid mechanics of waste-water disposal in the ocean. *Annu. Rev. Fluid Mech.* **7** (1), 187–211.
- KURGANOV, A. & PETROVA, G. 2000 Central schemes and contact discontinuities. *ESAIM-Math. Model. Num.* **34**, 1259–1275.
- KURGANOV, A. & TADMOR, E. 2000 New high-resolution central schemes for nonlinear conservation laws and convection–diffusion equations. *J. Comput. Phys.* **160** (1), 241–282.

- LAX, P. D. 1973 *Hyperbolic Systems of Conservation Laws and the Mathematical Theory of Shock Waves*. Society for Industrial and Applied Mathematics.
- LINDEN, P. F. 2000 Convection in the environment. In *Perspectives in Fluid Mechanics* (ed. G. K. Batchelor, H. K. Moffatt & M. G. Worster), pp. 287–343. Cambridge University Press.
- LINDEN, P. F., LANE-SERFF, G. F. & SMEED, D. A. 1990 Emptying filling boxes: the fluid mechanics of natural ventilation. *J. Fluid Mech.* **212**, 309–335.
- LIST, E. J. 1982 Turbulent jets and plumes. *Annu. Rev. Fluid Mech.* **14** (1), 189–212.
- MORTON, B. R. 1959 Forced plumes. *J. Fluid Mech.* **5**, 151–163.
- MORTON, B. R. 1971 The choice of conservation equations for plume models. *J. Geophys. Res.* **76** (30), 7409–7416.
- MORTON, B. R., TAYLOR, G. & TURNER, J. S. 1956 Turbulent gravitational convection from maintained and instantaneous sources. *Proc. R. Soc. Lond. A* **234** (1196), 1–23.
- PAPANICOLAOU, P. N. & LIST, E. J. 1988 Investigations of round vertical turbulent buoyant jets. *J. Fluid Mech.* **195**, 341–391.
- PLOURDE, F., PHAM, M. V., KIM, S. D. & BALACHANDAR, S. 2008 Direct numerical simulations of a rapidly expanding thermal plume: structure and entrainment interaction. *J. Fluid Mech.* **604**, 99–123.
- PRIESTLEY, C. H. B. & BALL, F. K. 1955 Continuous convection from an isolated source of heat. *Q. J. R. Meteorol. Soc.* **81** (348), 144–157.
- ROUSE, H., YIH, C. S. & HUMPHREYS, H. W. 1952 Gravitational convection from a boundary source. *Tellus* **4** (3), 201–210.
- SCASE, M. M. 2009 Evolution of volcanic eruption columns. *J. Geophys. Res.* **114**, F04003.
- SCASE, M. M., ASPDEN, A. J. & CAULFIELD, C. P. 2009 The effect of sudden source buoyancy flux increases on turbulent plumes. *J. Fluid Mech.* **635**, 137–169.
- SCASE, M. M., CAULFIELD, C. P. & DALZIEL, S. B. 2006a Boussinesq plumes and jets with decreasing source strengths in stratified environments. *J. Fluid Mech.* **563**, 463–472.
- SCASE, M. M., CAULFIELD, C. P. & DALZIEL, S. B. 2008 Temporal variation of non-ideal plumes with sudden reductions in buoyancy flux. *J. Fluid Mech.* **600**, 181–199.
- SCASE, M. M., CAULFIELD, C. P., DALZIEL, S. B. & HUNT, J. C. R. 2006b Time-dependent plumes and jets with decreasing source strengths. *J. Fluid Mech.* **563**, 443–461.
- SCASE, M. M. & HEWITT, R. E. 2012 Unsteady turbulent plume models. *J. Fluid Mech.* **697**, 455–480.
- SCHMIDT, W. 1941 Turbulente Ausbreitung eines Stromes erhitzter Luft. *Z. Angew. Math. Mech.* **21** (6), 351–363 (in German).
- SHABBIR, A. & GEORGE, W. K. 1994 Experiments on a round turbulent buoyant plume. *J. Fluid Mech.* **275**, 1–32.
- SHRINIVAS, A. B. & HUNT, G. R. 2014 Transient ventilation dynamics induced by heat sources of unequal strength. *J. Fluid Mech.* **738**, 34–64.
- SLAWSON, P. R. & CSANADY, G. T. 1967 On the mean path of buoyant, bent-over chimney plumes. *J. Fluid Mech.* **28**, 311–322.
- SPARKS, R. S. J., BURSİK, M. I., CAREY, S. N., GILBERT, J., GLAZE, L. S., SIGURDSSON, H. & WOODS, A. W. 1997 *Volcanic Plumes*. Wiley.
- SPEER, K. G. & RONA, P. A. 1989 A model of an Atlantic and Pacific hydrothermal plume. *J. Geophys. Res.* **94** (C5), 6213–6220.
- STEVENS, B. 2005 Atmospheric moist convection. *Annu. Rev. Earth Planet. Sci.* **33** (1), 605–643.
- STRANEO, F. & CENEDESE, C. 2015 The dynamics of Greenland's glacial fjords and their role in climate. *Annu. Rev. Marine Sci.* **7** (1), 89–112.
- TURNER, J. S. 1986 Turbulent entrainment: the development of the entrainment assumption, and its application to geophysical flows. *J. Fluid Mech.* **173**, 431–471.
- VUL'FSON, A. N. & BORODIN, O. O. 2001 Self-similar propagation regimes of a nonstationary high-temperature convective jet in the adiabatic atmosphere. *J. Appl. Mech. Tech. Phys.* **42** (2), 255–261.
- WANG, H. & LAW, A. W.-K. 2002 Second-order integral model for a round turbulent buoyant jet. *J. Fluid Mech.* **459**, 397–428.

- WHITHAM, G. B. 1974 *Linear and Nonlinear Waves*. Wiley.
- WOODHOUSE, M. J., HOGG, A. J., PHILLIPS, J. C. & SPARKS, R. S. J. 2013 Interaction between volcanic plumes and wind during the 2010 Eyjafjallajökull eruption, Iceland. *J. Geophys. Res.* **118** (1), 92–109.
- WOODS, A. W. 1988 The fluid dynamics and thermodynamics of eruption columns. *Bull. Volcanol.* **50** (3), 169–193.
- WOODS, A. W. 2010 Turbulent plumes in nature. *Annu. Rev. Fluid Mech.* **42**, 391–412.
- YANNAPOULOS, P. C. 2006 An improved integral model for plane and round turbulent buoyant jets. *J. Fluid Mech.* **547**, 267–296.
- YU, H.-Z. 1990 Transient plume influence in measurement of convective heat release rates of fast-growing fires using a large-scale fire products collector. *Trans. ASME J. Heat Transfer* **112** (1), 186–191.
- ZELDOVICH, Y. B. 1937 The asymptotic laws of freely-ascending convective flows. *Zhur. Eksper. Teor. Fiz.* **7**, 1463–1465; (in Russian). English translation in *Selected Works of Yakov Borisovich Zeldovich*, (ed. J. P. Ostriker), vol. 1, 1992, pp 82–85. Princeton University Press.